PDGFRα signaling in cardiac fibroblasts modulates quiescence, metabolism and self-renewal, and promotes anatomical and functional repair

Naisana S. Asli[1,2,3,4,#], Munira Xaymardan[1,3,5,#], Elvira Forte[1,2,5], Ashley J. Waardenberg[1], James Cornwell[1,5], Vaibhao Janbandhu[1,2], Scott Kesteven[1], Vashe Chandrakanthan[1], Helena Malinowska[1], Henrik Reinhard[1], Sile F. Yang[7], Hilda A Pickett[7], Peter Schofield[8], Daniel Christ[2,8], Ishtiaq Ahmed[1], James Chong[1], Corey Heffernan[1], Joan Li[1], Mary Simonian[3], Romaric Bouveret[1,2], Surabhi Srivastava[9], Rakesh K. Mishra[9], Jyotsna Dhawan[9,10], Robert Nordon[6], Peter Macdonald[1,2], Robert M. Graham[1,2], Michael Feneley[1,2], Richard P. Harvey[1,2,5,11*]

[1] Victor Chang Cardiac Research Institute, Darlinghurst, NSW 2010, Australia

[2] St. Vincent's Clinical School, University of New South Wales, Kensington, NSW 2052, Australia

[3] School of Dentistry, Faculty of Medicine and Health, University of Sydney, Westmead Hospital, Westmead, NSW 2145, Australia

[4] Sydney Medical School, Faculty of Medicine and Health, University of Sydney, Westmead Hospital, Westmead, NSW 2145, Australia

[5] Stem Cells Australia, Melbourne Brain Centre, The University of Melbourne, Victoria 3010, Australia

[6] Graduate School of Biomedical Engineering, University of New South Wales, Kensington, NSW 2052, Australia

[7] Telomere Length Regulation Unit, Children's Medical Research Institute, University of Sydney, Westmead, NSW 2145, Australia

[8] Garvan Institute of Medical Research, 384 Victoria Street, Darlinghurst, Sydney, NSW 2010, Australia

[9] Centre for Cellular and Molecular Biology, Uppal Rd. Hyderabad 500 007, India

[10] Institute for Stem Cell Biology and Regenerative Medicine, Bengaluru 560 065, India

[11] School of Biotechnology and Biomolecular Science, University of New South Wales, Kensington, NSW 2052, Australia

# These authors have equally contributed to this manuscript.

* Correspondence: r.harvey@victorchang.edu.au

SUMMARY

The interstitial and perivascular spaces of the mammalian heart contain a highly interactive tissue community essential for cardiac homeostasis, repair and regeneration. Mesenchymal cells (fibroblasts) are one of the most abundant cell types and make up the organ superstructure. They play key roles as sentinels, tissue architects, paracrine signaling hubs and lineage precursors, and are linked to heart disease through their roles in inflammation and fibrosis. Platelet-derived growth factors (PFGFs) are secreted by several cell types involved in cardiac injury and repair. Here we explore in detail how PDGF receptor α (PDGFRα) signaling in cardiac fibroblasts affects their activation, differentiation and self-renewal. Short-term systemic delivery of PDGF-AB to mice from the time of myocardial infarction (MI) led to activation, proliferation and increased self-renewal of fibroblasts, and subsequent expansion of myofibroblasts. Underpinning this, as evidenced in uninjured mice, was a cell cycle priming effect, in which PDGF-AB induced exit of fibroblasts from quiescence without stimulating proliferation. Despite fibrogenesis, however, treated MI hearts showed enhanced anatomical and functional repair that was associated with pro-regenerative effects on endothelial cells, immune cells and cardiomyocytes. Our study provides a rationale for a novel therapeutic approach to cardiac injury involving stimulating fibroblast activation and endogenous repair mechanisms.

Keywords: cardiac, heart, CFU-F, mesenchymal stem cell, stem cells, platelet-derived growth factor, PDGF, metabolism, myocardial infarction, heart regeneration.

INTRODUCTION

In humans, myocardial infarction (MI) is the most common form of acute cardiac injury leading to the death of millions of cardiomyocytes (CM), reduced heart function and high mortality. Therefore, achieving heart regeneration after MI is a major clinical imperative. The hearts of zebrafish and some urodele amphibia show spectacular regeneration though cardiomyocyte (CM) dedifferentiation and proliferation [1], and a similar capacity exists in neonatal mammalian hearts [2]. However, in the hearts of adult mammals, CM turnover is low [3] and replacement after MI is thought to be largely insignificant [4].

The heart also contains a variety of stromal cell types, including fibroblasts, myofibroblasts, cells forming the endocardium, epicardium, coronary and lymphatic vessels, nerves, as well as immune cells and potentially stem and progenitor cells, although a comprehensive understanding of this complex interacting cellular community is lacking. Fibroblasts are one of the most abundant cardiac cell types, acting as major sensing and signaling hubs through their progenitor, paracrine, mechanical and electrical functions [5-8], and are conspicuously linked to heart disease through their roles in inflammation and fibrosis. A common feature of regenerating tissues is that timely resolution of inflammation is critical for limiting fibrosis and allowing tissue replacement [9]. In the cardiac injury context, inhibition of fibrosis can lead to better functional recovery [10], but can predispose to cardiac rupture [11].

In the mouse, after MI, stromal fibroblasts are known to proliferate and differentiate into myofibroblasts, which stabilize the infarct through secretion of a collagen-rich matrix [8]. Myofibroblasts exist only transiently and are replaced in permanent scar by “matrifibrocytes” – senescent cells of fibroblast origin sharing expression signatures with osteoblasts and chondrocytes [12]. Depleted fibroblasts may be renewed during the injury process [13]. However, the mechanistic underpinnings of expansion, differentiation and renewal of fibroblast are poorly understood, although they may be governed by stem cell principles [14-16].

We have previously defined a population of cardiac clonal colony-forming cells (termed colony forming units - fibroblast; cCFU-F) that express the cell surface

markers SCA1 and PDGFRα, and that exhibit stem cell qualities, including long-term self-renew and multi-lineage differentiation capacity *in vitro*, akin to those of bone marrow (BM) mesenchymal stem cells (MSCs) [14, 16]. In the BM context, accumulating evidence show that subsets of cells enriched for CFU-F and *in vitro* multi-lineage differentiation properties, indeed correspond to *in vivo* multipotent lineage progenitors [17]. A potentially analogous population in skeletal muscle supports satellite stem cell activation, and gives rise to fibro-adipogenic cells in pathology [18]. We hypothesize that cCFU-F represent endogenous cardiac fibroblasts with self-renewal capacity, although how they contribute to homeostasis and repair as progenitors or through sentinel and paracrine functions, remains unclear.

To investigate the molecular regulation of the stromal cell hierarchy, we screened for receptor tyrosine kinases that were active in self-renewing cCFU-F cultures. Among the positives were the platelet-derived growth factor (PDGF) receptors. In mammals, there are 4 PDGF ligands, which form 5 heterodimeric species (AA, AB, BB, CC, DD) that bind with different affinities to homo- and/or heterodimers of the two cognate receptors (αα, αβ, ββ). This signaling system has been implicated in proliferation, migration and differentiation of a variety of mesenchymal cell types [19]. In the heart, PDGF-B/PDGFRβ signaling is involved in coronary angiogenesis in both development and adult stress responses [20], whereas PDGFRα is expressed by fibroblasts and its chronic activation leads to fibrosis [21]. However, the roles of PDGF signaling in the heart are complex and experimental manipulation can lead to diverse outcomes. For example, inhibition of PDGFRs can cause lethal cardiomyopathies [22], whereas delivery of PDGF-B ligand after MI can either induce fibrosis or improve cardiac repair [23, 24]. Thus, the therapeutic potential of modulating PDGF/PDGFR signaling *in vivo* remains unclear.

Here, we investigate a role for PDGFRα signaling in cardiac repair. Short-term delivery of PDGF-AB to mice from the time of MI led to enhanced proliferation of a sub-fraction of the fibroblast pool and expansion of myofibroblast numbers. Despite fibrogenesis, however, treated hearts showed enhanced anatomical and function repair. Underlying these effects, PDGFRα signaling stimulated exit of fibroblasts and cCFU-F from quiescence through modulation of their metabolic and self-renewal

states. Direct or paracrine effects on endothelial cells, monocytes and cardiomyocytes were identified, that likely contribute to enhanced cardiac repair. Taken together, our results highlight a pro-regenerative role for PDGFRα in the complex cellular interactions occurring during recovery of cardiac tissue from damage.

RESULTS

Modulation of PDGFR signaling in vitro

To identify pathways responsible for growth and self-renewal of cardiac fibroblasts, we tested the activity of 39 receptor tyrosine kinases (RTKs) in mouse cCFU-F cultures using an anti-phospho-tyrosine antibody array (Fig. S1A). Active PDGFRα/β, EGFR, ERBB2/4, AXL, MSPR, VEGFR3 and MUSK were identified. Here we chose to explore the function of PDGFRα in stromal cell and cCFU-F biology in greater detail.

We first modulated PDGFRα signaling in cardiac fibroblasts *in vitro*. In uninjured hearts, there are two major fibroblasts sub-sets - those expressing stem cell markers, SCA1 and PDGFRα (S^+P^+ cells), and those expressing PDGFRα but not SCA1 (S^-P^+ cells) (Fig. S1B). Only the S^+P^+ population forms colonies, thus linking cCFU-F to the $SCA1^+$ sub-set [14, 16].

Using live imaging and single cell lineage tracking, we determined that ~60% of freshly plated S^+P^+ cells (P0) underwent division in both generation (gen) 0 (those whose birth was not observed) and generations 1 to 4 (denoted >0; Fig. 1A). In gen 0, PDGF-AB strongly stimulated the probability (rate) of cell cycle entry and the overall proportion of the total cell population dividing (Fig. 1B), and also stimulated EdU incorporation over the first 24 hrs (Fig. 1C) and increased total cell yield at P0 (Fig. 1D). However, the small molecule PDGFRα/β inhibitor, AG1296, had no significant effect on the probability of cell division or the proportion gen 0 cells dividing (Fig. 1B). Paradoxically, however, there was a decrease in EdU incorporation with AG1296 treatment, as well as a decrease in cell number at the end

of P0 (Fig. 1C,D; see below), without changes in cell death (Fig. S1C). In gens >0, PDGF-AB also stimulated the probability of cell division, but to a lesser extent than in gen 0, whereas AG1296 decreased the probability of cell division (Fig. 1B). Western blotting showed reciprocal changes in cell cycle regulators, including Rb, p130, cyclins G1 and D1, and the cyclin-dependent kinase inhibitor $p27^{kip1}$ (Fig. 1E).

We repeated these experiments on cCFU-F cultures at P4, when cells were fully activated from quiescence (see below). After re-plating, 100% of cells divided in gen 0 and ~80% in gens >0 (Fig. 1A), although neither PDGF-AB nor inhibitor showed any significant impact on the probability of cell division or the proportion of cells dividing (Fig. 1F). However, EdU incorporation and total cell number were increased by PDGF-AB and decreased by the inhibitor by the end of P4 (Fig. 1G,H), with no change in cell death (Fig. S1D), and reciprocal changes in cell cycle regulators, as observed in treated P0 cells (Fig. S1E). Because the effects on EdU incorporation and cell yield cannot be explained by a change in the rate of cell division (ie. cell cycle length), we hypothesized that PDGFR signaling was having an impact on the dynamics of self-renewal.

Impact of modulating PDGF signaling on cCFU-F self-renewal

Around 1 in 120 S^+P^+ cells form large colonies in our cCFU-F assay [14]. We have previously shown using *in vitro* single cell tracking of cCFU-F pedigrees derived from *Pdgfa*$^{GFP/+}$ mice that only GFP^+ cells within colonies are capable of self-renewal (probability of self-renewing division >0.5), and do so mostly by symmetrical division [25]. We have also shown that the size of cCFU-F colonies reflects their clonal growth characteristics. Large colony cells can undergo self-renewal over many passages *in vitro* (>300 days), whereas small colonies show limited self-renewal (Chong et al. 2011), and micro-colony cells are composed almost exclusively of differentiated myofibroblast-like cells that are PDGFRα^- [25]; the latter rarely divide (Fig. S1F) and do not form secondary (2°) colonies (Chong et al., 2011). Thus, cardiac fibroblasts show a spectrum of colony-forming states, with a sub-population of cells within large colonies showing long-term self-renewal ability *in vitro*.

To explore the impact of altered PDGF signaling on colony formation, S^+P^+ cells were isolated from healthy adult hearts and cultured in the cCFU-F assay with and without increasing doses of PDGF ligand and/or AG1296 inhibitor, with large colonies being scored at the end of the first passage (P0; day 12). Among PDGF ligands tested (AA, AB, BB), PDGF-AB was the most potent in stimulating colony formation (data not shown), so we used it in further experiments. PDGF-AB has a preference for PDGFRα/α and PDGFRα/β dimers [26]. PDGF-AB increased the number of large colonies in a dose-dependent manner (Fig. 1I), and cell yield (Fig. 1D), whereas AG1296 decreased the number of large colonies and cell yield. As noted, PDGF-AB also stimulated EdU uptake, whereas AG1296 inhibited it (Fig. 1C). Addition of increasing amounts of a specific ligand-blocking PDGFRα monoclonal antibody (mAb) produced the same colony profile as increasing doses of AG1296 (Fig. S1G), confirming the involvement of PDGFRα in colony formation and growth.

We next asked whether the loss of colony-formation in PDGFR inhibitor-treated cells reflected permanent changes in cell state, for example commitment to differentiation. We cloned large, small and micro colonies from inhibitor and vehicle-treated P0 cultures, and clone pools were re-plated without inhibitor (Fig. 1I), continuing this clonal analysis through 2°, tertiary (3°) and quaternary (4°) assays (Fig. S1H). All inhibitor-treated colony types gave rise to large 2° colonies and further clonal passage restored large colony forming capacity to that typical of vehicle-treated large colonies (Fig. S1H), demonstrating that the loss of self-renewal with inhibitor is reversible. Importantly, in the presence of the inhibitor, bulk S^+P^+ cell cultures could be passaged continuously without exhaustion (>120 days/P13); however, these cultures showed a lower rate of self-renewal than vehicle-treated controls, whereas PDGF-AB ligand stimulated a higher rate of self-renewal (Fig. 1K).

Short-term PDGF-AB treatment promotes heart repair

To test directly whether the observed effects of PDGF-AB on cardiac fibroblast activation *in vitro* have any relevance to heart repair *in vivo*, we delivered PDGF-AB via mini-pump to wild-type (WT) mice over 5 days from the time of myocardial infarction (MI). This led to a ~40% increase in serum PDGF-AB levels (Fig. S2A). At

28 days post-MI, PDGF-AB-treated hearts showed reduced scarring and normalized heart/body weight ratio (Fig. 2A-C). Echocardiographic analysis revealed that ejection fraction (EF) was substantially improved at both day 5 and day 28 post-MI in PDGF-AB compared to PBS-treated hearts (Fig. 2D). Left ventricular (LV) fractional area change (FAC) was also improved at the ventricular apex which, in MI+PBS hearts, was virtually akinetic (Fig. 2E,F; Fig. S2B). PDGF-AB treatment also significantly improved LV end systolic (ES) and end diastolic (ED) areas at day 5 and 28 post-MI at all four short-axis echocardiographic planes surveyed (Fig. 2G,H; Fig. S2C,D).

We surveyed angiogenesis in treated hearts and found that PDGF-AB increased BrdU uptake in $CD31^+$ vascular endothelial cells (ECs) in both sham and MI hearts (Fig. 2I). After MI, there was an increase in total vascularity in remote as well as border and infarct zones, and in vessel caliber within the scar (Fig. 2J,K). These findings suggest that PDGF-AB can targets ECs directly [27]. The relative number of pro-inflammatory m1 monocytes was decreased at day-5 (Fig. S3E,F), leading to an increase in the $Ly\text{-}6C^{low}/Ly\text{-}6C^{high}$ (m2/m1) monocyte ratio (Fig. 2L) that reflects a pro-reparative monocyte milieu [5]. PDGF-AB also led to a ~6-fold increase in EdU incorporation in CMs at day 28, that was localized to cells around the LV cavity (Fig. S2G).

Impact of PDGF-AB on fibroblast proliferation and expansion in vivo

Based on these findings, we assessed fibroblast cell cycle re-entry and self-renewal *in vivo* using *Pdgfra*$^{nGFP/+}$ knockin mice that express a nuclear-localized fusion between histone H2B and eGFP [14]. Because of the stability of H2B-GFP, it can serve as a short-term lineage tag (see below). In sham hearts, virtually all S^+P^+ fibroblasts were GFP^{high}, as assessed by flow cytometry (Fig. 3A, left panel). The $SCA1^-$ fraction of fibroblasts (which do not form colonies) was also mostly GFP^{high} (S^-GFP^{high} cells; Fig.S3A). GFP^{high} cells were distributed throughout the myocardial interstitium, close to $isolectin^+$ microvessels, as well as in the *tunica adventia* of arterioles, consistent with previous studies of fibroblast distribution [8], but neither CMs nor ECs showed detectable GFP (Fig 3B-D). GFP^{high} cells were embedded within an adventitial-type collagen VI matrix (Fig. 3E) and were low for PDGFRβ and negative for other

pericyte markers, including CD146 (differing from other MSC populations [17]) and NG2 (Fig. 3F-H; Fig. S3B). Furthermore, all GFP^{high} cells were exclusively external to the collagen IV^{+} vascular basal lamina (Fig. 3I; 1500 cells scored), confirming that cardiac cCFU-F/MSC-like cells are not pericytes, a previous notion overturned recently [27].

Pdgfra-*GFP^{medium}* cells are cardiac myofibroblasts

In *Pdgfra*-GFP hearts post-MI, there was progressive accumulation of GFP^{medium} cells in both $SCA1^{+}$ and $SCA1^{-}$ fibroblast sup-fractions (Fig. 3A; Fig. S3A). These were negative for the blood lineage marker CD45 (Fig. S3C), and by day 5 post-MI most had become negative for surface PDGFRα (Fig. 3A). We determined that $S^{+}GFP^{medium}$ cells were enriched in myofiboblasts using a number of criteria, for example, qRT-PCR showed higher expression of myofibroblast markers in $S^{+}GFP^{medium}$ cells relative to $S^{+}GFP^{high}$ cells, including a ~70-fold increase in *Acta2* (encoding αSMA) (Fig. 3J) (see also Fig. S3D-F and legend). $S^{+}GFP^{medium}$ cells were also seen when cardiac fibrosis was induced by aldosterone/salt or aortic banding (Fig. 3K).

We confirmed that GFP^{high} cells give rise to the GFP^{medium} myofibroblasts by genetic lineage tracing of $PDGFR\alpha^{+}$ cells using tamoxifen (tam)-inducible *Pdgfra$^{merCremer/+}$* CRE recombinase driver mice crossed to a *Rosa26^{TdTomato}* CRE-reporter (Fig. 3L). Fourteen days after tam treatment and 5 days post-sham, tagged cells were $PDGFR\alpha^{bright}\alpha SMA^{-}$, typical of quiescent fibroblasts. Post-MI, however, the infarct region contained abundant, large, lineage-tagged $PDGFR\alpha^{dim}\alpha SMA^{high}$ myofibroblasts. These findings are consistent with other recent lineage tracing studies [12, 28, 29].

Using *Pdgfra*-GFP mice, we assessed BrdU uptake and cell flux over a 5-day period post-sham or MI. PDGF-AB was delivered continuously from the time of MI with BrdU via mini-pump (Fig. 4A) and for some of these *in vivo* experiments we also delivered the PDGFRα/β inhibitor, Imatinib, by oral gavage. In hearts from sham-operated mice, delivery of PDGF-AB did not increase BrdU incorporation in $S^{+}GFP^{high}$ or S^{-}

GFP^{high} cells, indicating that PDGF-AB has no mitogenic effect on cardiac fibroblasts in the absence of injury (Fig. 4A; Fig. S4A). In the context of MI, PDGF-AB induced a ~2-fold increase in BrdU incorporation in the $S^{+}GFP^{high}$ population but not the $S^{-}GFP^{high}$ population (Fig. 4A; Fig. S4A), showing differences between these populations in their responses to PDGF-AB.

GFP^{medium} myofibroblasts showed higher BrdU incorporation than GFP^{high} fibroblasts, likely as most had previously divided [12] (Fig. 4A; Fig.S4A). However, PDGF-AB did not stimulate a higher proportion of BrdU incorporation in GFP^{medium} myofibroblasts. Overall, PDGF-AB was mitogenic for injury-activated $S^{+}GFP^{high}$ fibroblast, but not for $S^{-}GFP^{high}$ fibroblasts or myofibroblasts, highlighting the specificity of its action within fibroblasts subsets.

Fibroblast and myofibroblast cell flux in PDGF-AB-treated MI hearts

To extend the above findings, we quantified changes in the number of fibroblasts and myofibroblasts after modulating PDGFR signaling *in vivo*. The $S^{+}GFP^{medium}$ myofibroblast population was absent in Sham+PDGF-AB hearts (Fig. 4B), indicating that exogenous PDGF-AB does not induce myofibroblast differentiation or expansion in the absence of injury. As shown above, in animals subjected to MI but not treated with PDGF-AB, GFP^{medium} myofibroblasts accumulated by 5 days post-MI (Figs. 3A; Fig. S3A) and this was inhibited by Imatinib (Fig. 4B) or by injection of blocking anti-PDGFRα antibody (Fig. S4B), showing that myofibrogenesis is at least partly dependent on endogenous PDGFRα signaling.

Strikingly, PDGF-AB induced a ~50% increase in the number of $S^{+}GFP^{medium}$ myofibroblasts by day 5 post-MI (Fig. 4B). $S^{-}GFP^{medium}$ myofibroblasts were not increased. Immunostaining showed a higher density of αSMA^{high} myofibroblasts throughout the infarct region in PDGF-MI hearts and these were GFP^{dull} (Fig. 4C), in line with their GFP^{medium} status in flow cytometry. Induced myofibroblasts expressed higher levels of calponin than those in MI+PBS hearts (Fig. S4C), perhaps indicating a distinct contractile state. Formation of GFP^{medium} myofibroblasts occurred at the expense of GFP^{high} fibroblasts in both $SCA1^{+}$ and $SCA1^{-}$ subfractions, and (for

SCA1$^+$ cells) in both MI+PBS and MI+PDGF hearts (Fig. 4B; Fig. S3A), showing that fibroblasts are depleted during the early phases of repair (see Discussion).

Cell cycle and biosythetic profiling of cardiac fibroblasts

We next profiled the cell cycle and metabolic status of relevant fibroblast populations using DNA (7AAD) and RNA (Pyronin Y) dyes and flow cytometry. Pyronin Y staining largely reflects ribosomal RNA and ribosomal protein mRNA content, and, thus, serves as a surrogate marker of the biosynthetic state of cells [30]. In uninjured and sham-operated hearts, virtually all freshly isolated S^+P^+ cells had 2n DNA content and 60% of cells exhibited a very low RNA state, typical of quiescence (G_0) (Fig. 5A). The remainder showed a continuum of higher biosynthetic states. With MI, however, there was a significant reduction in the proportion of cells in G_0 to ~40%, showing that a large number of quiescent fibroblasts become metabolically activated after MI (likely those in the peri-infarct region). Activation was completely inhibited by Imatinib treatment, demonstrating that this response involves PDGFR signaling.

Many long-lived stem cell populations exist in quiescence. To examine the biosynthetic state of cCFU-F, S^+P^+ cells were further fractionated to CD90$^+$PDGFRβ^{low} cells, which resulted in a >10-fold enrichment in large colony forming capacity (data not shown). Selection for SCA1-, PDGFRα- and CD90-expressing cells also enrich for CFU-F in adult murine BM [17]. Virtually all cells in the enriched cCFU-F fraction were in G_0 (Fig. 5A, lower panels), suggesting that cCFU-F are quiescent. Greater than 50% of these G_0 fibroblasts became metabolically active after MI, and this was partially inhibited by Imatinib. In agreement with these findings, cell cycle profiling on S^+P^+ fibroblasts from *Pdgfra*-GFP mice revealed a similar heterogeneous pattern of biosynthetic stages (Fig. 5B). S^+GFP^{medium} myofibroblasts also showed a continuum of biosynthetic states, although very few were in G_0 (~10%).

Impact of modifying PDGFRα signaling in uninjured hearts

We next asked if PDGF-AB or Imatinib had an effect on fibroblasts in the absence of injury. We found that in animals treated *in vivo* with PDGF-AB for 5 days, large colony formation was increased, whereas Imatinib treatment severely inhibited colony formation (Fig. 5C). Imatinib also significantly inhibited long-term fibroblast self-renewal (Fig. 5D). PDGF-AB partially mitigated the effects of Imatinib. These colony profiles closely resemble those obtained by treatment of cultured S^+P^+ cells with ligand/inhibitor (Fig. 1I,K). An identical outcome was seen after injection of blocking PDGFRα mAb (Fig. S5A,B). Importantly, whereas Imatinib had no impact on the proportion of S^+P^+ fibroblasts in G_0 in uninjured hearts, PDGF-AB decreased the number of G_0 cells by ~35% (Fig. 5E), supporting the notion that it has an important priming effect.

Cell cycle profiling of cCFU-F cultures in vitro

We also profiled the cell cycle in cCFU-F cultures using the PyroninY/7AAD assay. When freshly isolated S^+P^+ cells were cultured until the end of P0, ~46% of cells remained in G_0 (Fig. 5F). Because 60% of P0 cells divide after plating (Fig. 1A), many of these dividing cells must retain or re-assume a low biosynthetic state. This delayed adaption to cell culture likely accounts for the slower rate of self-renewal of cCFU-F cultures up until P4 (48 days) [14] (Figs. 1M, 5D) and is consistent with the slow activation of stem cells from quiescence [31]. Strikingly, cultures treated with PDGF-AB ligand showed a decrease in the proportion of cells in G_0 from ~46% to ~29% (Fig. 5F), whereas AG1296 increased the proportion of cells in G_0 from 46% to ~81%. Even in P4 cultures, where virtually all cells were metabolically active ($RNA^{medium\text{-}high}$) (Fig. 5G), treatment with AG1296 led to ~50% of cells being drawn into G_0, with an associated reduction in cell yield (Fig. 1H).

Exit from PDGFRα-inhibition-induced quiescence requires AKT and cMYC

To understand whether these biosynthetic changes correlated with other metabolic indicators, we probed mitochondrial and metabolic signaling pathways. Using MitoTracker Red, we found that PDGF-AB increased the proportion with higher mitochondrial mass, whereas AG1296 increased the proportion of cells with a lower

mass (Fig. 6A). These effects were accompanied by changes in transcripts encoding mitochondrial polymerases (POLG, POLG2) and the transcription factor, TFAM (Fig. 6B).

PDGFRα signaling is known to activate the PI3K/AKT/FOXO pathway involved in cell growth, metabolism and stem cell function [32, 33]. Treatment of cCFU-F cultures with PDGF-AB until the end of P0 activated the AKT and cMYC pathways, as seen by increases in the active phosphorylated forms of AKT (pAKT473, pAKT308) and in AKT-dependent phosphorylation of FOXO (which excludes it from the nucleus and marks it for degradation), as well as in increased cMYC levels (Fig. 6C). Conversely, AG1296 led to a decrease in pAKT and pFOXO, and an increase in total FOXO, consistent with induction of quiescence [33].

If inhibitor-treated P4 cultures were released from inhibitor for a further passage (P5) there was an induction of a hyper-metabolic state with only ~1% of cells remaining in G_0 (condition AG-R versus control; Fig. 6E; Fig. S6A). Time course Western blot analysis of AG-R cultures across P5 showed increased levels of pAKT and cMYC (Fig. 6D). Exploiting this assay, we asked if the AKT and cMYC pathways were required for exit from the G_0 state imposed by PDGFR inhibition. At the concentrations used, neither the AKT inhibitor (LY294002) nor cMYC inhibitor (10058-F4) had any impact on steady state growth or the cell cycle profile of control cultures (Fig. S6B,C; data not shown). However, exit from the G_0 state induced by PDGFR inhibition was blocked in a dose-dependent manner by both drugs (Fig. 6E,F). Thus, PDGFR signaling inhibition in cCFU-F cultures imposes a low metabolic/proliferative state resembling quiescence, release from which requires AKT and cMYC.

Trancriptome analysis of treated cCFU-F cultures

Microarray transcriptome and principal component analysis of cultured cCFU-F at P0 showed that inhibitor-treated cells were transcriptionally distinct from those of untreated and ligand-treated cultures, which clustered together (Fig. 7A). The top gene ontology (GO) terms associated with genes downregulated by inhibitor were

nucleosome assembly (driven largely by down-regulation of histone genes), as well as *epigenetic regulation of gene expression*, *DNA methylation*, *cell proliferation*, *migration* and *adhesion*, *negative regulation of apoptosis*, and angiogenic and other signaling pathways (Fig. 7B; Table 1), all consistent with a repressed proliferative, transcriptional and epigenetic state in inhibitor-treated cultures.

There were also many genes up-regulated with inhibitor, associated with terms for *cell adhesion* and *extracellular matrix*, as well as *negative regulation of Wnt signaling* and a variety of tissue developmental processes (Fig. 7B), consistent with findings that quiescence involves active states controlling metabolism, proliferation and differentiation [34].

Overall, our studies demonstrate a role for PDGFRα signaling in modulating exit of fibroblasts from quiescence, and their activation and proliferation, and highlight the potential of manipulating these parameters therapeutically.

DISCUSSION

Replacing CMs lost to ischemic injury will be necessary for achieving heart regeneration in humans. However, the diverse stromal populations of the heart, which form a complex interactive cellular community contributing to organ architecture, viability and function, will also need to be restored in parallel [13]. In pro-regenerative animals, fibroblasts, vessels, immune cells and nerves are all essential for heart regeneration [35]. Understanding and unlocking the paracrine signaling activities and pro-regenerative functions of these cells is therefore a research and therapeutic priority.

PDGFs have been implicated as mitogens for mesenchymal cells and MSCs, and chronic activation of PDGFR signaling has been associated with fibrosis and cancer in different settings [21]. Attempts at modulating PDGFR signaling after MI have led to diverse outcomes, from improved heart repair after MI to frank heart failure in uninjured mice [23, 36, 37]. These studies highlight the lack of a mechanistic understanding of how PDGFR signaling regulates the different aspects of heart

repair, and the therapeutic potential of altering PDGFR signaling *in vivo* remains unclear.

Here we investigated the role of PDGFRα signaling in the cardiac fibroblast compartment using a variety of approaches to measure cell flux, exit from quiescence, proliferation, metabolism, self-renewal and differentiation. The most significant impact of augmented PDGFRα signaling was to increase the metabolic state of quiescent fibroblasts and promote their exit from G_0. In particular, this was reflected by an increase in the probability of cell cycle entry *in vitro*, and in the proportion of cardiac fibroblasts exiting G_0 in uninjured hearts. As a consequence, PDGF-AB treatment from the time of MI led to profound changes in fibroblast activation, proliferation and differentiation to myofibroblasts.

We have mapped for the first time the metabolic state and flux in cardiac fibroblasts *in vitro* and *in vivo*. In uninjured hearts, fibroblasts exist in a continuum of metabolic/biosynthetic states with around half in G_0/quiescence. Like other stem cell populations present in uninjured adult mice, cCFU-F were exclusively in quiescence. After MI, a significant proportion of quiescent fibroblasts (~30%) exited G_0 and became activated. Importantly, even in the absence of injury, *in vivo* PDGF-AB treatment enhanced exit of fibroblasts from quiescence without stimulating DNA synthesis, and this was accompanied by increased formation of large colonies. These finding demonstrate the priming effect of PDGF-AB in uninjured hearts.

Pdgfra$^{GFP/+}$ knock-in mice allowed us to distinguish numerous fibroblast sub-populations based on the level of expression of GFP and other markers, and to follow their behavior and fate during heart repair. The majority of fibroblasts (including activated fibroblasts) are GFP^{high}, consistent with previous studies demonstrating that most fibroblasts in uninjured hearts express PDGFRα [38], whereas GFP^{medium} cells were identified as myofibroblasts. Using PDGFR inhibitors and a specific PDGFRα blocking antibody, we found that PDGFRα signaling was essential to activate both fibroblasts and cCFU-F from quiescence, post-MI. PDGFRα signaling was also essential for the full transition of activated fibroblasts to myofibroblasts. We have shown that PDGF-AB promotes activation and proliferation of fibroblasts after MI, but

is not mitogenic for myofibroblasts, likely due to the down-regulation of PDGFRα in these cells (Fig. 3A). Thus, we hypothesize that the impact of PDGFRα on fibrogenesis relates to its early priming role on fibroblasts, which stimulates their proliferation in the context of injury-induced mitogens. PDGFs are expressed by numerous cell types associated with cardiac injury and could rapidly prime the surviving stroma. While it is possible that some fibroblasts differentiate directly to myofibroblasts without proliferation, recent work shows that most myofibroblasts undergo at least one cell division [12], suggesting that fibroblast differentiation may be coupled to proliferation.

Manipulation of PDGFRα signaling *in vitro* supported the above model. In freshly plated S^+P^+ cells, PDGF-AB treatment led to an increased probability of cell cycle re-entry over the first few cell cycles, and, subsequently, increased metabolism, colony formation and self-renewal, without apparent effects on the rate of proliferation, or commitment to differentiation. PDGFR inhibition had the opposite effect. These findings extend previous work showing that PDGF acts as a *competence* factor during re-entry of serum-starved fibroblasts to the cell cycle [39]. The primed state of PDGF-AB-induced fibroblasts may have similarities to G(Alert), a reversible, activated state induced in skeletal muscle stem cells by remote injury [31]. In common with G(Alert), PDGF-AB-primed S^+P^+ fibroblasts showed an increased rate of cell cycle re-entry *in vitro*. However, concomitant changes in cell size, mitochondrial content and activation of the AKT/mTOR pathway were not observed in S^+P^+ cells after PDGF-AB-treatment or ischemic preconditioning (induced by hind limb ischemic injury) (Fig. S5C-E), albeit that effects on minor populations of cells (eg. cCFU-F) may have been masked.

PDGFRα blockade in both freshly plated and P4 S^+P^+ cells inhibited cell cycle re-entry and induced a reversible low metabolic/biosynthetic akin to quiescence. This was accompanied by decreased colony formation and rate of self-renewal. Exit from this state required AKT and cMYC, which are known to be involved in G_0/G_1 checkpoint control. Inhibition led to altered expression of cell cycle regulators and to profound changes in the transcriptome. Down-regulation in the expression of epigenetic pathways after PDGFRα inhibition suggests that the induced quiescence

is accompanied by rearrangement of chromatin architecture, as seen in endogenous stem cell populations [40]. In addition to down-regulated genes, hundreds of genes were up-regulated in PDGFRα-inhibited cells, consistent with findings that maintenance of quiescence involves active programs [34]. The quiescence induced in cCFU-F cultures *in vitro* by PDGFR inhibition may resemble the quiescent state observed in ~50% of GFP^+ fibroblasts in healthy hearts. Consistently, when we inhibited PDGFRα signaling in uninjured hearts, there was a decrease in colony formation and the rate of self-renewal *ex vivo* was strongly and permanently inhibited. Thus, PDGFRα signaling is necessary for maintaining cCFU-F metabolic and niche characteristics *in vivo*.

Overall, our studies suggest that a dynamic continuum of cell states underpins stromal fibroblast behavior, proliferation and lineage differentiation. The graded spectrum of colony forming ability, self-renewal and metabolism reflects this continuum. Different matrix and vascular niche environments likely set up the continuum, which could be influenced by hypoxic, signaling or biomechanical gradients. Our studies reinforce the link between metabolism, and stem and progenitor cell states, and suggest that a proportion of cardiac fibroblasts have stem cell-like properties. It is noteworthy that GFP^{high} fibroblasts became depleted during MI (either by cell death or differentiation), highlighting the need for their renewal for effective repair [13]. Our ongoing single cell RNA sequencing studies demonstrates the phenomenon of fibroblast renewal after MI (data not shown), although how this occurs and whether it is dependent on self-renewal of fibroblasts requires further analysis.

Treatment of MI hearts with PDGF-AB led to a ~50% increase in the number of GFP^{medium} myofibroblasts, which occupied the infarct and border zones. We hypothesize that metabolic priming accelerates the transition of stromal cells to activated states, and their response to injury-induced mitogens and differentiation factors, such as ROS, TGFβ, ANG2, ET-1 and immune cytokines [41]. An entirely unexpected finding was that, despite robust induction of myofibrogenesis, PDGF-AB treated MI hearts showed significantly enhanced repair from 5 days post-MI. Salutary effects included a 50% reduction in scar volume, normalization of heart weight/body

weight ratio, and improvements in ejection fraction as well as end systolic and diastolic volumes. Even though we did not readily detect GFP^+ ECs in uninjured *Pdgfra*-GFP hearts, PDGF-AB increased BrdU uptake in ECs of both sham and MI hearts, and increased vascular density in infarct, boarder and remote zones of MI hearts, suggesting direct effects of PDGF-AB on ECs. PDGFRα expression has been reported previously in a sub-fraction of endothelial cells in uninjured hearts [42]. PDGF-AB also induced a 4-5-fold increase in EdU incorporation into CMs and an increase in m2/m1 monocyte ratio. Given the severity of infarcts imposed in this mouse study (mean EF ~20%), the degree of functional improvement is noteworthy, and would be highly significant in the clinical setting. Noting the different levels of calponin expression in myofibroblasts of PDGF-AB-treated MI hearts, we speculate that altered secretion and/or remodeling of matrix leads to improved chamber compliance.

There remains a strong clinical and economic case for the development of new regenerative therapies including modulators of fibrosis, and indeed several existing cardiac standard-of-care drugs, such as statins, act, in part, as anti-fibrotics [5]. Our study demonstrates the diverse pro-regenerative impacts that can be achieved by targeting the cardiac fibroblast hierarchy.

Of note, in contrast to previous efforts to effect regeneration by expansion, characterization and implantation of various cell populations; cellular reprogramming that is of low efficiency and involves the use of viral vectors; complex direct intra-myocardial or trans-coronary administration of various pro-regenerative factors, or surgical application of bioengineered cell sheets, the potential to stimulate repair post injury, non-invasively, by the simple parenteral administration of a factor, such as PDGF-AB, that may activate endogenous pro-regenerative responses, is clinically attractive. This is particularly the case in the post-MI setting when invasive interventions are poorly tolerated, and are likely to limit the translatability of many therapeutic pro-regenerative approaches currently under evaluation.

Author Contributions

N.S.A., M.X., V.C. and R.P.H conceived of the study; All authors designed and conducted experiments, analyzed data and contributed to the paper; R.P.H, R.M.G., M.F. and R.N. provided supervision; RPH provided financial support; N.S.A., M.X. and R.P.H. wrote the paper.

Acknowledgements

We acknowledge support from the Australian Stem Cell Centre (P082, S4M1), Australia India Strategic Research Fund (BF020084, BF050024), Australian Research Council Strategic Initiative in Stem Cell Science (SR110001002), Australian Academy of Science Visiting Scholar's Program, Foundation Leducq Transatlantic Networks of Excellence in Cardiovascular Research (13CVD01, 15CVD03), New South Wales Cardiovascular Research Network (100711), James Kirby Foundation, and National Health and Medical Research Council of Australia (NHMRC; 354400, 573732, 1074386). RPH held an Australia Fellowship and Senior Principal Research Fellowship from the NHMRC (573705, 1118576).

References

1. Kikuchi K, Holdway JE, Werdich AA, Anderson RM, Fang Y, Egnaczyk GF, Evans T, Macrae CA, Stainier DY and Poss KD. Primary contribution to zebrafish heart regeneration by gata4(+) cardiomyocytes. *Nature*. 2010;464:601-5.

2. Porrello ER, Mahmoud AI, Simpson E, Hill JA, Richardson JA, Olson EN and Sadek HA. Transient regenerative potential of the neonatal mouse heart. *Science*. 2011;331:1078-80.

3. Bergmann O, Zdunek S, Felker A, Salehpour M, Alkass K, Bernard S, Sjostrom SL, Szewczykowska M, Jackowska T, Dos Remedios C, Malm T, Andra M, Jashari R, Nyengaard JR, Possnert G, Jovinge S, Druid H and Frisen J. Dynamics of Cell Generation and Turnover in the Human Heart. *Cell*. 2015;161:1566-75.

4. Eschenhagen T, Bolli R, Braun T, Field LJ, Fleischmann BK, Frisen J, Giacca M, Hare JM, Houser S, Lee RT, Marban E, Martin JF, Molkentin JD, Murry CE, Riley PR, Ruiz-Lozano P, Sadek HA, Sussman MA and Hill JA. Cardiomyocyte Regeneration: A Consensus Statement. *Circulation*. 2017;136:680-686.

5. Gourdie RG, Dimmeler S and Kohl P. Novel therapeutic strategies targeting fibroblasts and fibrosis in heart disease. *Nature reviews Drug discovery*. 2016;15:620-38.

6. Shinde AV and Frangogiannis NG. Fibroblasts in myocardial infarction: a role in inflammation and repair. *Journal of Molecular and Cellular Cardiology*. 2014;70:74-82.

7. Tallquist MD and Molkentin JD. Redefining the identity of cardiac fibroblasts. *Nature Reviews Cardiology*. 2017;14:484-491.

8. Travers JG, Kamal FA, Robbins J, Yutzey KE and Blaxall BC. Cardiac Fibrosis: The Fibroblast Awakens. *Circulation research*. 2016;118:1021-40.

9. Mescher AL. Macrophages and fibroblasts during inflammation and tissue repair in models of organ regeneration. *Regeneration (Oxf)*. 2017;4:39-53.

10. Kaur H, Takefuji M, Ngai CY, Carvalho J, Bayer J, Wietelmann A, Poetsch A, Hoelper S, Conway SJ, Mollmann H, Looso M, Troidl C, Offermanns S and Wettschureck N. Targeted Ablation of Periostin-Expressing Activated Fibroblasts Prevents Adverse Cardiac Remodeling in Mice. *Circulation research*. 2016;118:1906-17.

11. Oka T, Xu J, Kaiser RA, Melendez J, Hambleton M, Sargent MA, Lorts A, Brunskill EW, Dorn GW, 2nd, Conway SJ, Aronow BJ, Robbins J and Molkentin JD. Genetic manipulation of periostin expression reveals a role in cardiac hypertrophy and ventricular remodeling. *Circulation research*. 2007;101:313-21.

12. Fu X, Khalil H, Kanisicak O, Boyer JG, Vagnozzi RJ, Maliken BD, Sargent MA, Prasad V, Valiente-Alandi I, Blaxall BC and Molkentin JD. Specialized fibroblast differentiated states underlie scar formation in the infarcted mouse heart. *Journal of Clinical Investigation*. 2018;128:2127-2143.

13. Kanisicak O, Khalil H, Ivey MJ, Karch J, Maliken BD, Correll RN, Brody MJ, SC JL, Aronow BJ, Tallquist MD and Molkentin JD. Genetic lineage tracing defines myofibroblast origin and function in the injured heart. *Nature communications*. 2016;7:12260.

14. Chong JJ, Chandrakanthan V, Xaymardan M, Asli NS, Li J, Ahmed I, Heffernan C, Menon MK, Scarlett CJ, Rashidianfar A, Biben C, Zoellner H, Colvin EK, Pimanda JE, Biankin AV, Zhou B, Pu WT, Prall OW and Harvey RP. Adult cardiac-resident MSC-like stem cells with a proepicardial origin. *Cell stem cell*. 2011;9:527-40.

15. Cornwell JA, Nordon RE and Harvey RP. Analysis of cardiac stem cell self-renewal dynamics in serum-free medium by single cell lineage tracking. *Stem Cell Research*. 2018;28:115-124.

16. Noseda M, Harada M, McSweeney S, Leja T, Belian E, Stuckey DJ, Abreu Paiva MS, Habib J, Macaulay I, de Smith AJ, al-Beidh F, Sampson R, Lumbers RT, Rao P, Harding SE, Blakemore AI, Jacobsen SE, Barahona M and Schneider MD. PDGFRalpha demarcates the cardiogenic clonogenic Sca1+ stem/progenitor cell in adult murine myocardium. *Nature communications*. 2015;6:6930.

17. Kfoury Y and Scadden DT. Mesenchymal cell contributions to the stem cell niche. *Cell Stem Cell*. 2015;16:239-53.

18. Heredia JE, Mukundan L, Chen FM, Mueller AA, Deo RC, Locksley RM, Rando TA and Chawla A. Type 2 innate signals stimulate fibro/adipogenic progenitors to facilitate muscle regeneration. *Cell*. 2013;153:376-88.

19. Andrae J, Gallini R and Betsholtz C. Role of platelet-derived growth factors in physiology and medicine. *Genes and Development*. 2008;22:1276-312.

20. Chintalgattu V, Ai D, Langley RR, Zhang J, Bankson JA, Shih TL, Reddy AK, Coombes KR, Daher IN, Pati S, Patel SS, Pocius JS, Taffet GE, Buja LM, Entman ML and Khakoo AY. Cardiomyocyte PDGFR-beta signaling is an essential component of the mouse cardiac response to load-induced stress. *Journal of Clinical Investigation* 2010;120:472-84.

21. Olson LE and Soriano P. Increased PDGFRalpha activation disrupts connective tissue development and drives systemic fibrosis. *Developmental cell*. 2009;16:303-13.

22. Savi M, Frati C, Cavalli S, Graiani G, Galati S, Buschini A, Madeddu D, Falco A, Prezioso L, Mazzaschi G, Galaverna F, Lagrasta CAM, Corradini E, De Angelis A, Cappetta D, Berrino L, Aversa F, Quaini F and Urbanek K. Imatinib mesylate-induced cardiomyopathy involves resident cardiac progenitors. *Pharmacology Research*. 2018;127:15-25.

23. Gallini R, Lindblom P, Bondjers C, Betsholtz C and Andrae J. PDGF-A and PDGF-B induces cardiac fibrosis in transgenic mice. *Experimenal Cell Research*. 2016;349:282-290.

24. Hsieh PC, MacGillivray C, Gannon J, Cruz FU and Lee RT. Local controlled intramyocardial delivery of platelet-derived growth factor improves postinfarction ventricular function without pulmonary toxicity. *Circulation*. 2006;114:637-44.

25. Cornwell JA, Hallett RM, der Mauer SA, Motazedian A, Schroeder T, Draper JS, Harvey RP and Nordon RE. Quantifying intrinsic and extrinsic control of single-cell fates in cancer and stem/progenitor cell pedigrees with competing risks analysis. *Scientific reports*. 2016;6:27100.

26. Heldin CH and Lennartsson J. Structural and functional properties of platelet-derived growth factor and stem cell factor receptors. *Cold Spring Harbor perspectives in biology*. 2013;5:a009100.

27. Edelberg JM, Aird WC, Wu W, Rayburn H, Mamuya WS, Mercola M and Rosenberg RD. PDGF mediates cardiac microvascular communication. *The Journal of clinical investigation*. 1998;102:837-43.

28. Ivey MJ, Kuwabara JT, Pai JT, Moore RE, Sun Z and Tallquist MD. Resident fibroblast expansion during cardiac growth and remodeling. *Journal of Molecular and Cellular Cardiology*. 2018;114:161-174.

29. Moore-Morris T, Guimaraes-Camboa N, Banerjee I, Zambon AC, Kisseleva T, Velayoudon A, Stallcup WB, Gu Y, Dalton ND, Cedenilla M, Gomez-Amaro R, Zhou

B, Brenner DA, Peterson KL, Chen J and Evans SM. Resident fibroblast lineages mediate pressure overload-induced cardiac fibrosis. *Journal of Clinical Investigation*. 2014;124:2921-34.

30. Kozma SC and Thomas G. Regulation of cell size in growth, development and human disease: PI3K, PKB and S6K. *Bioessays*. 2002;24:65-71.

31. Rodgers JT, King KY, Brett JO, Cromie MJ, Charville GW, Maguire KK, Brunson C, Mastey N, Liu L, Tsai CR, Goodell MA and Rando TA. mTORC1 controls the adaptive transition of quiescent stem cells from G0 to G(Alert). *Nature*. 2014;510:393-6.

32. Demoulin JB and Essaghir A. PDGF receptor signaling networks in normal and cancer cells. *Cytokine & growth factor reviews*. 2014;25:273-83.

33. Tothova Z, Kollipara R, Huntly BJ, Lee BH, Castrillon DH, Cullen DE, McDowell EP, Lazo-Kallanian S, Williams IR, Sears C, Armstrong SA, Passegue E, DePinho RA and Gilliland DG. FoxOs are critical mediators of hematopoietic stem cell resistance to physiologic oxidative stress. *Cell*. 2007;128:325-39.

34. Chen BR, Cheng HH, Lin WC, Wang KH, Liou JY, Chen PF and Wu KK. Quiescent fibroblasts are more active in mounting robust inflammatory responses than proliferative fibroblasts. *PLoS One*. 2012;7:e49232.

35. Vivien CJ, Hudson JE and Porrello ER. Evolution, comparative biology and ontogeny of vertebrate heart regeneration. *NPJ Regenerative Medicine*. 2016;1:16012.

36. Zymek P, Bujak M, Chatila K, Cieslak A, Thakker G, Entman ML and Frangogiannis NG. The role of platelet-derived growth factor signaling in healing myocardial infarcts. *Journal of the American College of Cardiology*. 2006;48:2315-23.

37. Gallini R, Huusko J, Yla-Herttuala S, Betsholtz C and Andrae J. Isoform-Specific Modulation of Inflammation Induced by Adenoviral Mediated Delivery of Platelet-Derived Growth Factors in the Adult Mouse Heart. *PLoS One*. 2016;11:e0160930.

38. Ivey MJ and Tallquist MD. Defining the Cardiac Fibroblast. *Circulation Journal*. 2016;80:2269-2276.

39. Jones SM and Kazlauskas A. Growth-factor-dependent mitogenesis requires two distinct phases of signalling. *Nature Cell Biology*. 2001;3:165-72.

40. Cheung TH and Rando TA. Molecular regulation of stem cell quiescence. *Nature reviews Molecular cell biology*. 2013;14:329-40.

41. Morry J, Ngamcherdtrakul W and Yantasee W. Oxidative stress in cancer and fibrosis: Opportunity for therapeutic intervention with antioxidant compounds, enzymes, and nanoparticles. *Redox Biology*. 2017;11:240-253.

42. Edelberg JM, Lee SH, Kaur M, Tang L, Feirt NM, McCabe S, Bramwell O, Wong SC and Hong MK. Platelet-derived growth factor-AB limits the extent of myocardial infarction in a rat model: feasibility of restoring impaired angiogenic capacity in the aging heart. *Circulation*. 2002;105:608-13.

Figure Legends

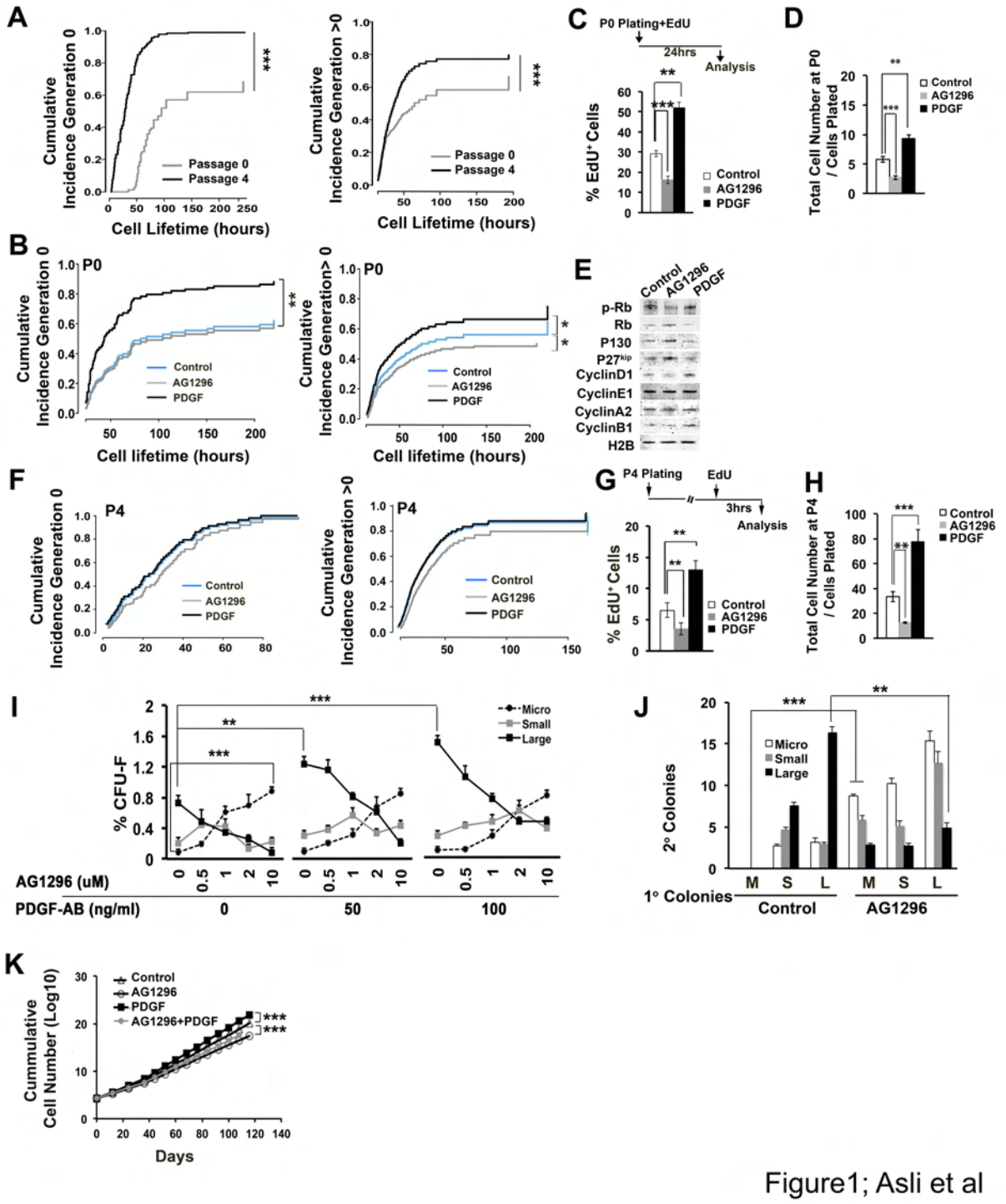

Figure1; Asli et al

Figure 1: Role of PDGFRa signaling in cCFU-F cultures

(A) Accumulated proportion of cells undergoing division over time (cumulative index) in freshly plated S^+P^+ cells across P0, and cCFU-F cultures re-plated at the end of P4, scored separately in generation 0 (whose birth was not observed) and generations >0. (B) Single cell analysis of cumulative cell division in freshly plated S^+P^+ cells with and without PDGF-AB and AG1296, scored separately in generations 0 and >0. (C) EdU incorporation in S^+P^+ cultures (24hr pulse, then analysis at the

end of P0). (D) Total cell number in cCFU-F cultures treated with vehicle (control), AG1296 (10μM) or PDGF-AB (100ng/ml) scored at the end of P0 (see Fig. 1I). (E) Western blot analysis of indicated cell cycle regulators in S^+P^+ cultures at P0. (F) Live cell tracking analysis of the accumulated proportion of cells undergoing division over time across P4 cells treated with vehicle, AG1296 or PDGF-AB, scored separately in generation 0 and generations >0. (G,H) Total cell number and EdU incorporation, respectively, arising from treatment of cCFU-F cultures across P4 with AG1296 or PDGF-AB. (I) Colony analysis (large, small, micro-colonies) in S^+P^+ cells scored at P0 (day 12), with and without indicated concentrations of PDGF-AB ligand and PDGFR signaling inhibitor AG1296. (J) Secondary (2^0) colony formation assaying pooled cloned primary large, small and micro-colonies from untreated control and AG1296-inhibited (10μM) cultures as in panel I (see Fig. S1H for continuing 3^0 and 4^0 analyses). (K) Long-term cultures of S^+P^+ cells with or without PDGF-AB (100ng/ml) and AG1296 (10μM). All comparisons: ** $p<0.01$; *** $p<0.001$.

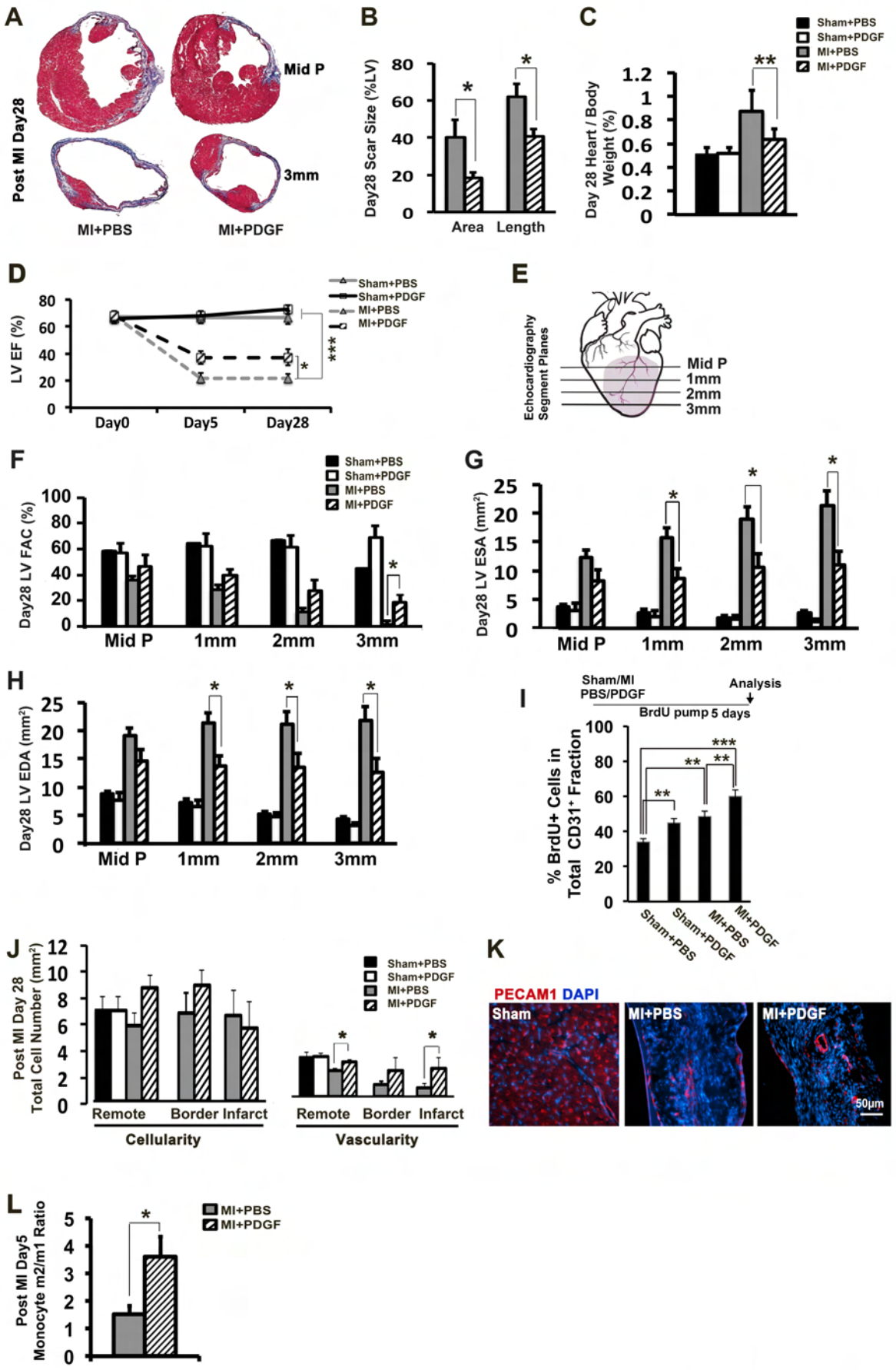

Figure2; Asli et al

Figure 2: PDGF-AB enhancement of cardiac anatomical and function repair in MI hearts

(A) Distribution of scar (Masson's Trichrome staining) in PBS and PDGF-AB-treated hearts 28 days post-MI at mid-papillary (Mid P) and 3 mm below Mid P levels (see Fig. 2E). (B) Scar area and length in PBS and PDGF-AB MI hearts. (C) Heart Weight/Body Weight ratio in day 28 sham/MI hearts. (D) LV ejection fraction (EF) in sham/MI hearts treated with PBS or PDGF-AB at 0 (baseline), 5 and 28 days. (E) Cartoon showing short axis planes for echocardiographic analyses. Mid P: mid-papillary. (F) Percent LV fractional area change (FAC) at different echocardiographic planes at day 28. (G,H) LV end systolic area (ESA) and diastolic area (EDA; panel L), respectively, at different echocardiographic planes at day 28. (I) BrdU uptake in $CD31^+$ endothelial cells in sham/MI hearts with PBS or PDGF-AB treatments. (J) Total cellularity (DAPI-stained nuclei/mm^3) and vascularity ($CD31^+$ micro-vessels/mm^3) in remote, boarder and infarct zones of day 28 sham/MI hearts. (K) Immunostaining showing increased caliber of $PECAM1^+$ vessels in the infarct zone of PDGF-AB-treated day 28 post-MI hearts. (L) Quantification of flow cytometric analysis of m2/m1 monocyte ratios in PBS and PDGF-AB-treated MI hearts at day 5. All comparisons: * $p<0.05$; ** $p<0.01$; *** $p<0.001$.

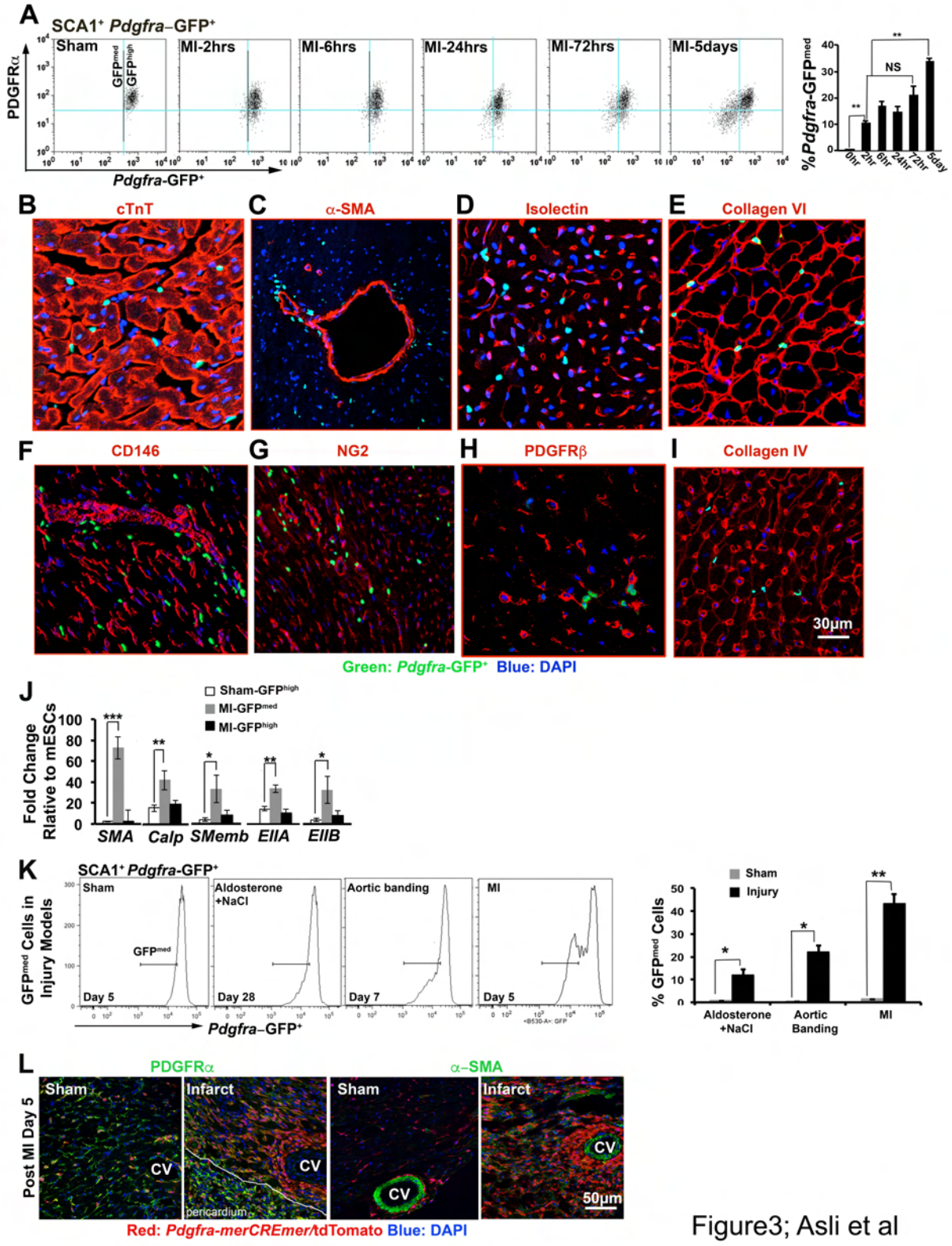

Figure 3: *In situ* localization of *Pdgfra*-GFP^{high} fibroblasts and appearance of *Pdgfra*-GFP*medium* myofibroblasts after MI

(A) Time course flow cytometry analysis of SCA1^{+}/*Pdgfra*-GFP^{+} fibroblasts, displaying PDGFRα and GFP expression, with quantification of GFP^{medium}

myofibroblasts. (B-I) Localization of *Pdgfra*-GFP^{+} fibroblasts in hearts sections of uninjured adult *Pdgfra*$^{GFP/+}$ knock-in mice relative to indicated markers detected by immunofluorescence: cTnT: cardiac troponin T; α-SMA: α-smooth muscle actin. (J) qRT-PCR analysis of myofibroblast markers in total GFP^{medium} and GFP^{high} cells at 5 days post-sham or MI. (K) Flow cytometry showing SCA1^{+}*Pdgfra*-GFP^{+} fibroblasts from *Pdgfra*$^{GFP/+}$ mice subjected to sham operation and disease models - aldosterone/high salt treatment, aortic banding, MI - with GFP^{medium} myofibroblast population (bar) quantified (see Fig. 4B). (L) Lineage tracing of PDGFRα fibroblasts at 5 days post-sham/MI, using tamoxifen-treated *Pdgfra*$^{merCREmer/+}$;*Rosa26*$^{tdTomato/+}$ mice and immunofluorescence for lineage trace (tdTomato), PDGFRα and SMA. Panels highlight lineage-positive fibroblasts that are PDGFRα^{bright} (sham) or PDGFRα^{dull} and SMA-positive (infarct). The *tunica media* of large coronary arteries is SMA^{bright}. First infarct panel - tdTomato^{+}PDGFRα^{bright} pericardium has adhered to the myocardium. cv: coronary vessel. All comparisons: * $p<0.05$; ** $p<0.01$; *** $p<0.001$.

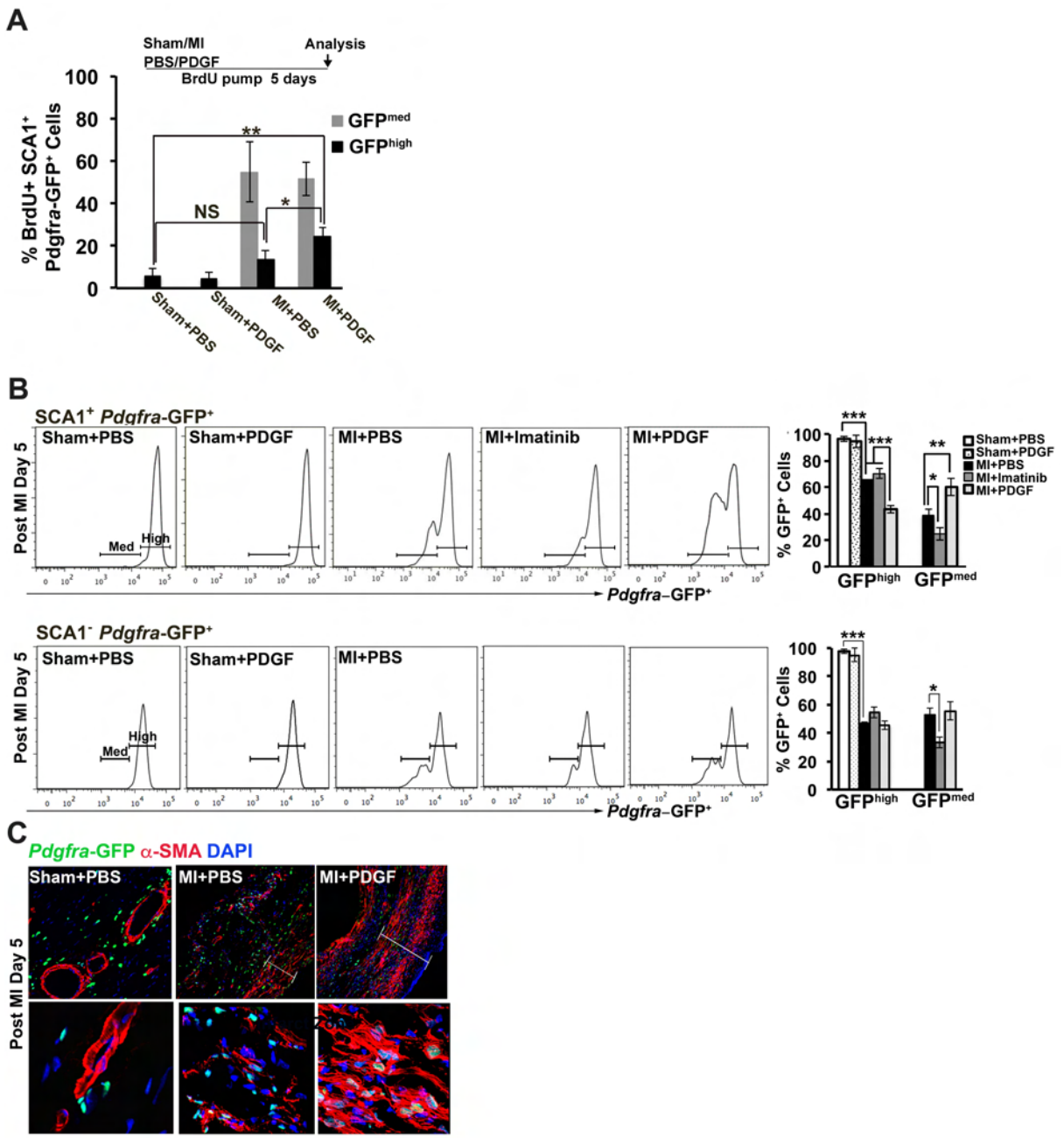

Figure 4: Analysis of proliferation and cell flux in the fibroblast lineage in sham/MI hearts with PDGF-AB and Imatinib treatments

(A) Accumulated BrdU incorporation in GFP^{high} fibroblasts and GFP^{medium} myofibroblasts in hearts at 5 days post-sham/MI after treatment with PBS or PDGF-AB. (B) Flow cytometry quantifying GFP^{high} fibroblasts (High) and GFP^{medium} myofibroblasts (Med) from day 5 post-sham/MI hearts treated with PBS or PDGF-AB in both SCA1^{+} SCA1^{-} fibroblast sub-fractions. MI mice were also treated with

Imatinib. (C) Immunofluorescence showing *Pdgfra*-GFP^{+} and SMA^{+} cells in sham/MI mice treated with PBS or PDGF-AB. Brackets indicate GFP^{dull}SMA^{+} myofibroblasts within the infarct zone shown at higher power in lower panels. All comparisons: * $p<0.05$; ** $p<0.01$; *** $p<0.001$.

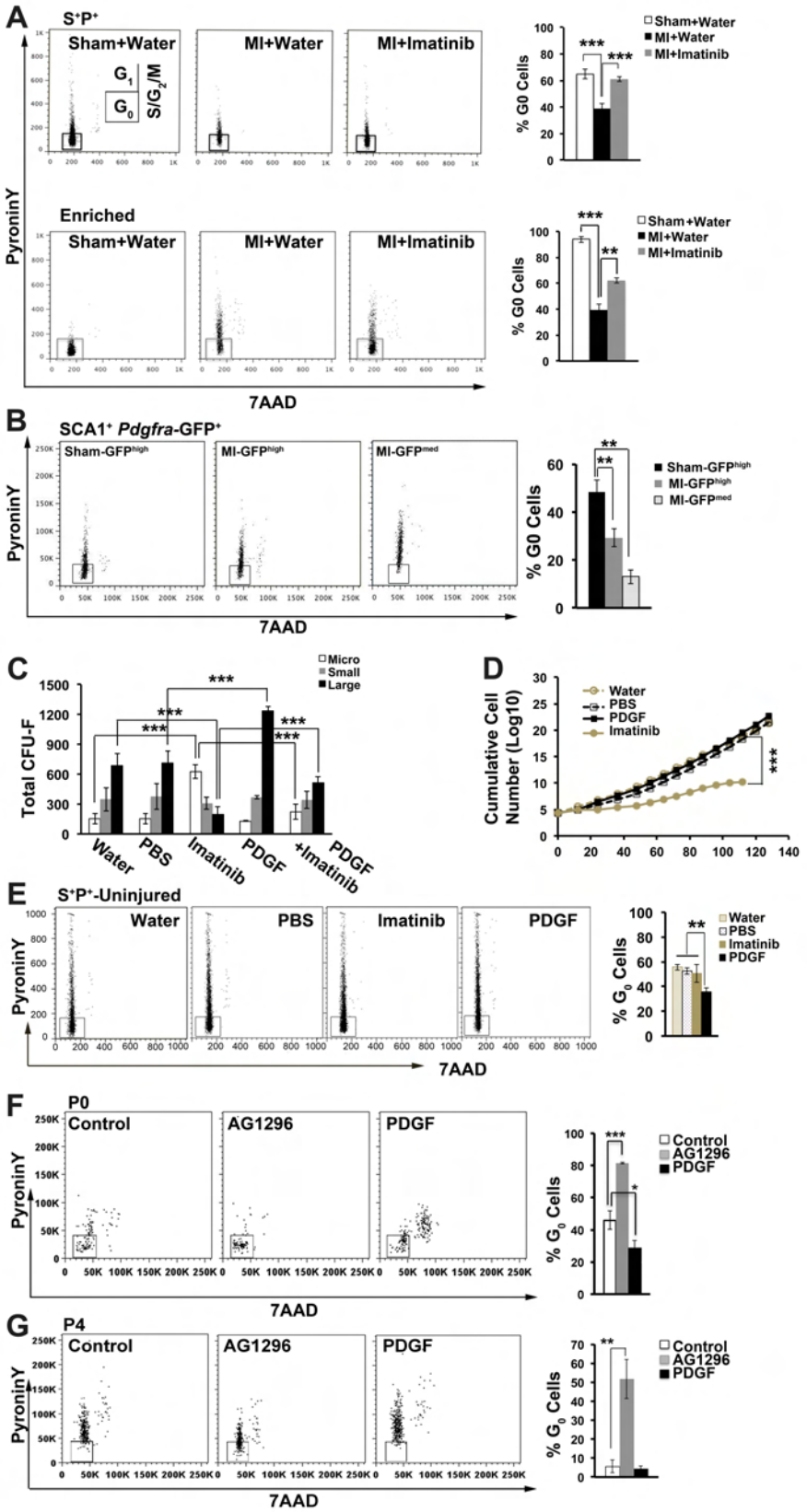

Figure5; Asli et al

Figure 5: Cell cycle, colony formation and growth analyses of fresh and cultured fibroblasts after PDGFRα ligand and inhibitor treatments

(A) PyroninY/7AAD cell cycle analyses of freshly isolated S^+P^+ and colony-enriched fibroblasts at day 5 post-sham/MI. Insert shows cell cycle compartments. Data also shown from MI mice treated with Imatinib or water control. Percent G_0 cells (boxed) indicated. (B) Cell cycle analysis of S^+*Pdgfra*-GFP^+ fibroblasts (flow-purified GFP^{high} and GFP^{medium} fractions) from *Pdgfra*$^{GFP/+}$ mice subject to sham/MI. Graph indicates percent G_0 cells (boxed). (C) cCFU-F analysis after *in vivo* treatment of uninjured mice with Imatinib and/or PDGF-AB ligand relative to vehicle controls at day 5. (D) Long-term growth curves of S^+P^+ cultures after *in vivo* treatments as indicated in (C). (E) PyroninY/7AAD cell cycle analysis of freshly isolated S^+P^+ cells from uninjured hearts treated as in A, with G_0 proportions graphed. (F) Cell cycle analyses of S^+P^+ cultures with and without PDGF-AB and AG1296 at P0. (G) Cell cycle analysis of P4 S^+P^+ cultures with and without AG1296 or PDGF-AB. All comparisons: * $p<0.05$; ** $p<0.01$; *** $p<0.001$.

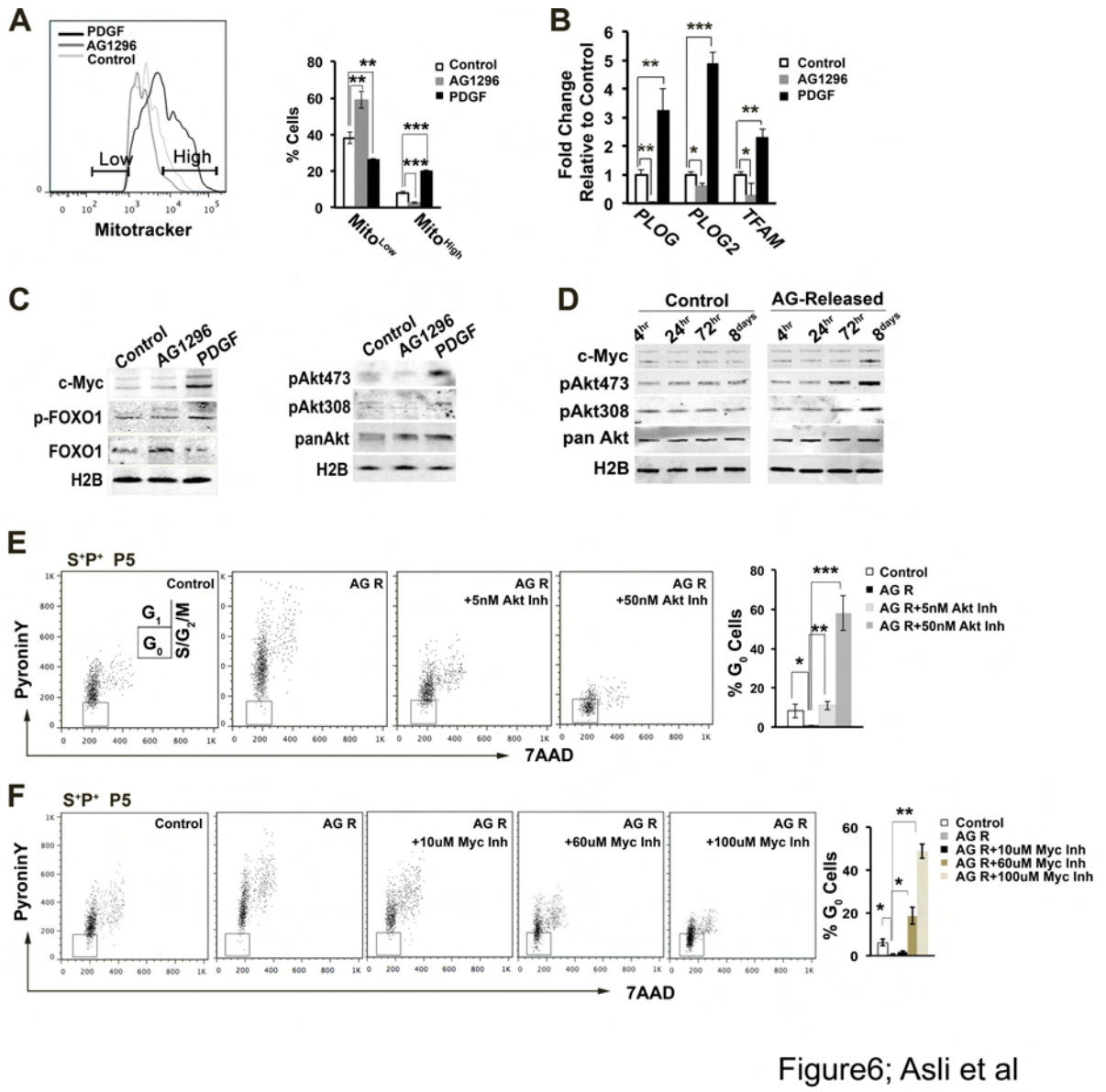

Figure6; Asli et al

Figure 6: Metabolic and cell cycle of S^+P^+ cultures – essential role of AKT and cMYC in cell cycle reentry after PDGFR inhibition

(A) Quantification of mitochondrial mass in S^+P^+ cells cultured to P0 by Mitotracker® Green FM (Mito) staining, with or without PDGF-AB (100ng/ml) and AG1296 (10μM), showing quantification of $Mito^{low}$ and $Mito^{high}$ fractions. (B) qRT-PCR analysis of genes for mitochondrial polymerase enzymes (POLG; POLG2) and transcription factor (TFAM). (C,D) Western blot analyses of indicated cMYC and AKT pathway proteins in PDGF-AB and AG1296-treated S^+P^+ cultures at P0 (C), and after AG1296 inhibition across P4 and release from inhibition for a further passage (AG-Released; D). (E,F) Cell cycle analysis of uninhibited cultures (P5) compared to cultures treated across P4 with AG1296 and released (AG R), with and without increasing doses of

AKT and cMYC inhibitors. Graphs in E and F show proportion of cells in G_0. All comparisons: * p<0.05; ** p<0.01; *** p<0.001.

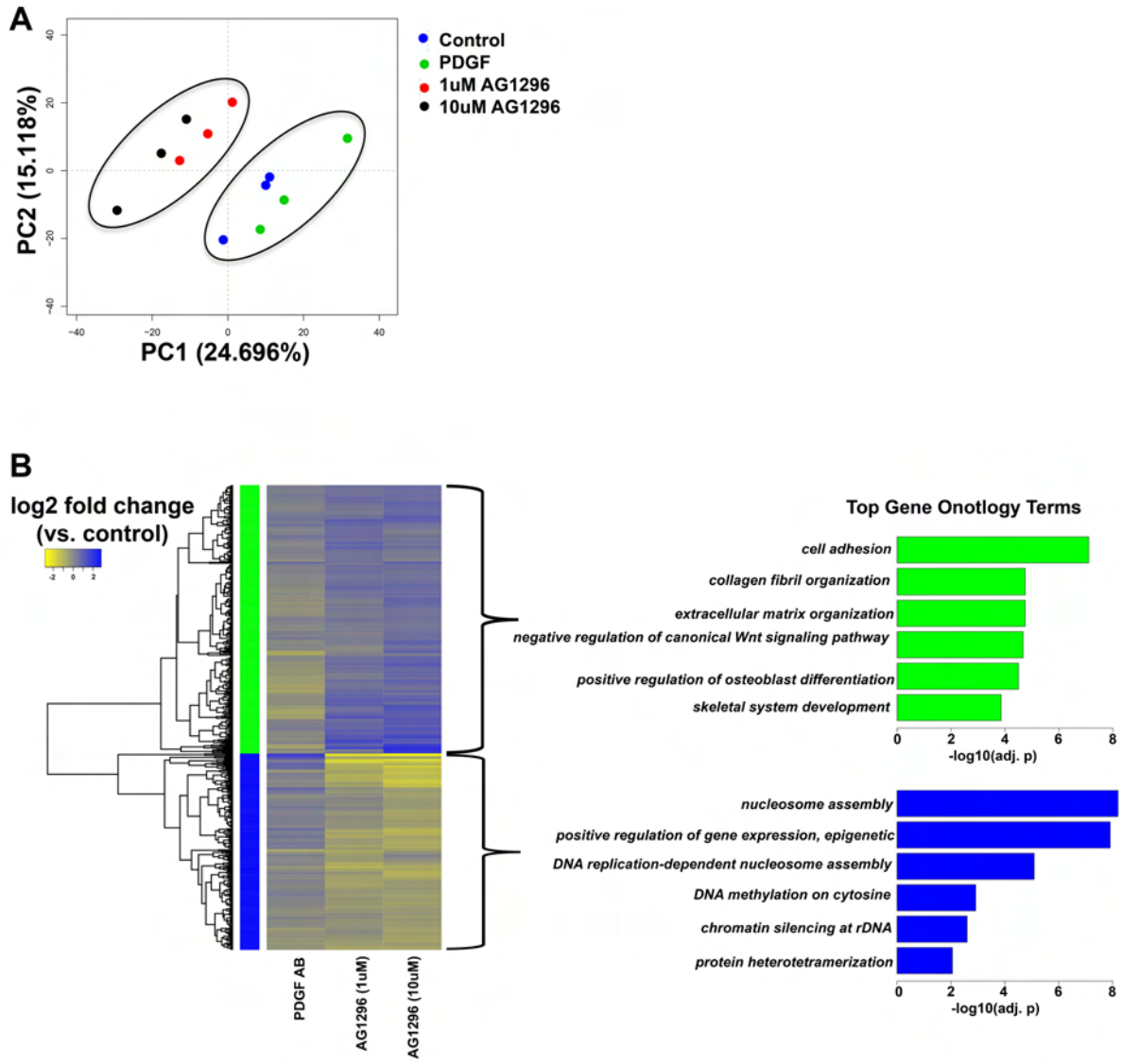

Figure 7: Transcriptome analysis of PDGF and AG1296-treated cultures

(A) Principal component (PC) analysis (PC1 vs PC2) of microarray transcriptome data from S^+P^+ cells cultured to P0 with and without PDGF-AB (100ng/ml) and AG1296 (1 and 10μM). (B) Heat map of differentially expressed genes (log2 ratio) between AG1296 (1μM), AG1296 (10μM), or PDGF-AB-treated cells versus untreated controls (adjusted p value <0.05); and top gene ontology terms for biological processes (benjamini adjusted p values) of the two distinguishing clusters (up-regulated and down-regulated with inhibitor compared to PDGF-AB-treated).

Supplementary Files List

1. **Detailed methods and materials**
2. **Supplementary figures and legend**
3. **References of the supplementary materials**
4. **Resources table (kits and reagents)**

1. Detailed Methods and Materials

EXPERIMENTAL MODEL AND SUBJECT DETAILS

***In vivo* animal studies:** All animal experiments were approved by the St Vincent's Hospital and Garvan Institute of Medical Research Animal Ethics Committee. Mice were bred and housed in the BioCORE facility of the Victor Chang Cardiac Institute. Rooms were temperature and light/dark cycle controlled. Standard food was provided *ad libitum*. Soggy and/or high nutrient food was provided after surgery.

Mouse strains used in experiments include C57Bl6J, *Pdgfra*-GFP, *Nkx2-5*-GFP, *Pdgfra*-merCremer and tdTomato (please see Key Resources Table for details). Both male and female mice aged 8-12 weeks (young) to 18-20 weeks (aged) were used. Surgical models included acute myocardial infarction (MI), catheterized minipump implantation, minipump implantation, tamoxifen treatment and oral gavage. Tissues were collected both from healthy and surgical mice for establishment of primary cell cultures, flow cytometry, immunohistochemistry and gene expression studies. Surgical procedures were performed in the BioCORE sugery suites between 9:30am to 3:30pm.

Primary cell culture: Primary cells were isolated from the mice and cultured at 37°C in 5% CO_2 and normoxia as described in relavent sections.

METHOD DETAILS

Cardiac CFU-F isolation and long term culture: Whole hearts were collected from mice that were either untreated, had undergone sham or MI surgeries, were treated with PDGF-AB ligand or vehicle via minipump and/or PDGFRa signaling inhibitor or vehicle via oral gavage, and cCFU-F assays performed as described in relevant sections. Once collected, hearts were minced and enzymatically digested as previously described [1]. The labeled cells were sorted by FACS for S^+P^+ population and plated at the density of 5000-cells/35cm^2 dish or 20,000 cells/75cm^2 flasks for long-term growth assays as described [1]. Colonies were scored as large, small and micro colonies according to their sizes following a crystal violet staining. For clonal analysis, the single large, small and micro-colonies were trypsinised within O-ring Cloning Cylinders (Corning), and then cells were pooled, centrifuged and plated separately. Cloned colony-derived cultures were then subjected to ligand/inhibitor treatments, differentiation assays, long-term or serial clone-based cultures as

described in relevant procedures. Bulk cultured cells were split every 12 days until passage 4, then every 8 days thereafter. Cumulative growth curves were plotted on a logarithmic scale, following standard cell number calculations. In brief, cumulative cell numbers for each passage comprised the total cell number harvested, multiplied by the previous cumulative number divided by number of cells plated.

***In vitro* treatment of ligands, inhibitors and monoclonal antibodies**

Bulk or clone cultures of flow-sorted cardiac S^+P^+ cells isolated from healthy hearts were treated with PDGF-AB (50ng/ml) ligand, PDGFRa/b chemical inhibitor AG1296 (0.5-10μM), AKT (5-50nM) or cMYC (10-100mM) inhibitors, or control or PDGFRa-blocking monocolonal IgGs (0.02-10mg/ml), adding the reagents to culture media and refreshing with each media change.

Cell cycle analysis, BrdU, EdU, TUNEL and mitochondrial assays

Cells sorted from mouse hearts with and without *in vivo* or *in vitro* treatments were used for cell cycle analysis. Staining of the cells with PyroninY and 7AAD was performed with minor modifications to the previously described method [2]. In brief, cells were fixed in ice-cold 80% ethanol and stored at -20^{0}C at least overnight. Cells were permeabilized by the Cytoperm Plus buffer (Becton Dickinson) for 5 mins and washed with 1x Cytoperm wash buffer before staining. Cellular DNA was stained with 7AAD (Becton Dickinson) and RNA with PyroninY (Sigma) before visualization by flow cytometry (Becton Dickinson CantoII). Data analysis was performed using FlowJo software. BrdU, EdU and TUNEL assays were performed using the APC-BrdU assay kit (Becton Dickinson), the Click-iT EdU assay kit (Thermofisher Scientific) and the DeadEnd™ Colorimetric TUNEL System (Promega), respectively, following manufacturers instructions. For mitochondrial assays, cells were harvested following standard methods, washed once with PBS and resuspended in culture medium containing 200nM of Mitotracker Green FM (Thermofisher Scientific). The staining mix was incubated for 15min at 37°C and analysed on a FACS CantoII (Becton Dickinson).

Live cell imaging and single-cell tracking of cCFU-F

Live cell imaging was performed using a Leica live cell imaging microscope (DMI6000B) equipped with x-y-z controller and hardware autofocus as described [3]. Phase contrast images were acquired every 15 minutes for 12 days (288 hours). Raw images were exported to Matlab for removal of background noise, enhancement of contrast, and to stitch contiguous frames of view using custom-written scripts. Custom-written software implemented in Matlab (Nordon's Tracking Tool) was used to manually track cell nuclei through consecutive frames, to build trajectories and record fate outcomes (division, death, and right censored [lost or not recorded]). At least 200 cells from at least 20 individual clones per condition were tracked from two separate wells. Statistical analyses of live cell tracking data were implemented in custom-written scripts in Matlab. Kaplan-Meier analysis was used to generate empirical cumulative distribution functions for cell division. Cox regression was used to test for group differences and to estimate the relative risk of division relative to untreated controls. The relative frequency of observed fates in each treatment group was quantified by counting the number of cells with distinct fate outcomes in each group. Student's *t*-tests were used to test for significant differences in the proportion of observed fates in each treatment group. All Matlab code will be made available upon request.

Quantitative RT-PCR, Western blots and receptor tyrosine kinase array
Quantitative RT-PCR, was performed using the SYBR master mix (Roche) following manufacturer's instructions. PCR reactions were run on LightCycler480 (Roche). Expression values were calculated using the Delta Ct method. Western blotting and immunocyto/histochemistry experiments were performed following standard protocols. For a comprehensive list of primers and antibodies used, refer to Key Resources Table. To profile active receptor tyrosine kinase pathways in cardiac CFU-F cultures, mouse phospho-RTK array kit was empolyed (R&D Systems) according to manufacturer's instructions. 100mg of total protein was added to each membrane.

Microarray sample preparation and analysis
For studies with inhibitor and ligand (P0) and on clonal small and large colonies (P5-P15), three independent experiments were performed for each condition. Total RNA was extracted using RNAeasy micro RNA isolation kit (Qiagen) and the quality of RNA was assessed using the Nanodrop (Thermofisher Scientific; 230/260>1.8, 260/280>1.8) and Bioanalyzer (Agilent, RIN>8.0). The RNA was further processed for microarray analysis by the Ramaciotti Center for Genomics (University of New South Wales, Sydney). Total RNA (100ng) of was labelled using the Affymetrix WT kit (Ambion). 3.52 mg of fragmented labelled ssDNA was hybridised to Mouse Gene 1.0 ST Gene Arrays for 16 hours at 45°C in the Affymetrix GeneChip Oven. Arrays were washed on the Affymetrix Fluidics 450 instrument as per manufacturer's protocol using the Affymetrix GeneChip Hybridization Wash & Stain kit for cartridge arrays. Arrays were scanned on the Affymetrix GeneChip 3000 7G Scanner instrument as per manufacturer's protocol and the Affymetrix GeneChip Command Console (AGCC) software was used to generate the CEL files from the DAT image files. RAW and normalised microarray data are available at NCBI's Gene Expression Omnibus (GSE106778; GSE106779) [4]

Microarray data were processed and analyzed in R/Bioconductor [5] Heatmaps were generated using the gplots R package and where clusters were identified, were split by cutting the tree at the reported height. Gene ontology analyses were performed using DAVID [6] gainst the *Mus musculus* background. Quality control was first performed using the 'affy' and 'affyPLM' R packages to assess the distribution of probe-level effects via the RLE and PLM methods as well as pseudoimage decomposition of the microarrays [7] No artefacts or outliers were revealed. Data were then normalised at the transcript level using Robust Multichip Average (RMA) normalisation. Principle component analysis was performed using the pcaMethods R package [8] using singular value decomposition. For determination of differentially expressed genes, a linear model with Bayes variance shrinkage was fit using the limma R package [9] to determine moderated t-statistics for all pair-wise comparisons. P-values were then corrected for multiple hypothesis testing using the Benjamini and Hochberg method [10]. Unless reported otherwise, a corrected p-value less than or equal to 0.05 was reported as significant. Where multiple probe sets were assigned to the same annotated gene, the gene with the highest average expression was reported for further analyses.

Immunohistochemistry and confocal microscopy in tissues
Cryosections (8µm) of paraformaldehyde (PFA; 4%) perfusion fixed and sucrose

treated hearts were cut and incubated with one or more primary antibodies overnight at 4°C (listed in Table S2) after incubating with a blocking solution including 1% bovine serum albumin, 3% serum (from the species that the secondary antibodies were derived), 0.03% triton X-100 in PBS for 30 minutes at room temperature. Nuclear counter-staining was performed after visualization of the markers by incubating sections with appropriate fluorochrome-conjugated secondary antibodies. EdU staining were performed on day 28 post-MI mouse hearts from animals treated with EdU+PDGF/PBS using a Click-iT EdU assay kit (Thermofisher Scientific) following manufacturer's instructions. Images were acquired using a Zeiss upright microscope or Zeiss confocal microscope.

Immunohistochemistry and confocal microscopy on cells

Cells were fixed with 4% PFA for 5 minutes at room temperature, washed with PBS and incubated with one or more primary antibodies for 1 hour at 4°C (listed in Table S2) after incubating with a blocking solution including 1% bovine serum albumin, 3% serum (from the species that the secondary antibodies were derived), 0.03% triton X-100 in PBS for 30 minutes at room temperature. Nuclear Hoechst counter-stains performed after visualization of the markers by incubating the sections with appropriate fluorochrome-conjugated secondary antibodies. Images were acquired by using a Zeiss upright microscope ot Zeiss confocal microscope.

Systemic delivery of ligands, inhibitors and monoclonal antibodies

PDGF-AB ligand (R&D, 20µg/ml) or vehicle (PBS) was administered systemically by a subcutaneous minipump (Alzet), inserted to the right external jugular vein via 13mm of 28G catheter (Alzet) through a 1mm incission. The ligand/vehicle was continuously released at a concentration of 0.5µl/hr for 5 days. Imatinib was delivered via oral gavage once daily at a concentration of 20mg/kg daily for 5 days. To block PDGFRa *in vivo,* mice were injected with one dose of 400ug (2mg/ul) on day 1, 200mg each on days 4 and 8, before either MI or sham surgeries.

Acute myocardial infarction

Mice were anaesthetised by intraperitoneal injection of ketamine (100mg/kg) and xylazine (20mg/kg), and intratracheally intubated. The hearts were exposed via a left intercostal incision, the left anterior descending coronary arteries were ligated just before the first diagonal branching point, lungs inflated and the wounds suture closed. Sham operations were performed without the ligation of the coronary artery. The mice were given intra-muscular injection of Bupernopherine for 3 days. Hearts were collected for immuno-histochemistry, FACS analysis or echocardiography 5-28 days after surgery as indicated for individual experiments.

Chronic cardiac injury models

Aldosterone mediated cardiac fibrosis: Anaesthetised mice were implanted with a 14 day mini-pump (Alzet 1002*)* containing either aldosterone (0.15mg/hr) or vehicle (polyethylene glycol) through a dorsal skin incision [11]. Mice were fed with water containing 1% NaCl**.** The osmotic pumps were replaced after 2 weeks and hearts analyzed on 28 days. Excess aldosterone generates hypervolemic hypertension and cardiac fibrosis by stimulating water and sodium reabsorption, and release of vasopressin [12].

Aortic banding assays: The aorta was exposed through a mediastinum incision in anaesthetised and intubated mice. The aortic root was isolated and a 4-0 constrictor suture was placed by using a template wire for diameter control. The incision was then closed and the animals recovered. Hearts were analysed at day 28 post surgery.

Echocardiography

Mice were anaesthesized using 5% isoflurane delivered by nose cone and echocardiography was performed on supine mice using a Vevo770 (Visualsonics Inc., Toronto, Canada) under 1-2% isoflurane on a warming pad set to 37°C. B-mode images were taken of the LV long axis (LAX) of the heart followed by four short axis (SAX) images, starting at the mid-papillary muscle level and at 1, 2 and 3mm towards the apex. Using Vevo770 Workstation software the following data were obtained by a blinded operator from the echocardiography images: LV length was measured from the apical dimple to the base of the aortic valve leaflets from the LAX images at end diastole (ED) and end-systole (ES). The areas boarded by the endocardium were planimetrically measured on all four SAX images at ED and ES, and from this a modified Bullet formula was used to derive ED and ES LV volumes (LVvol = L x (mean endocardial area) x 5/6).

Quantification of cellularity and vascularity

CD31 and DAPI stained sections of infarcted and sham-operated hearts were imaged using Zeiss 700 upright confocal microscope at 20 times magnification to cover entire left ventricle. Images were segmented as infarct, border and remote zones. The images were imported into the Image J to analyze total cell and vessels numbers in the respective areas.

Heart weight/body weight and infarct size measurement

Mice were weighed postmortem at post-surgical day 28, then hearts were resected and weighed sepately. Percentage heart weigh/body weight was calculated. Hearts were embedded in OCT and frozen. 10mM sections were stained using a Masson's Trichrome staining kit (Sigma) and stained slides were scanned using an Aperio ePathology scanner (Leica). The area size and lenth of the left ventricules were measured using Image J.

Flow cytometry analysis of immune cell influx and time course analysis of GFP^{medium} population

For immune influx analysis, the total interstitial population isolated by FACS was subjected to further fractionation with monocyte makers. Within the monocyte/macrophage population (CD45^{+} CD11b^{+} Ly-6G^{low}), type 1 monocytes (m1) were defined as Ly-6C^{high}[F4/80/I-A^{b}/CD11c]^{low}, and monocyte type 2 (m2) as Ly-6C^{low}[F4/80/I-A^{b}/CD11c]^{low} (see Fig. S6A,B). In time course analyses (2 hrs to 5 days), *Pdgfra*-GFP mice were used to separately quantify the *Pdgfra*-GFP^{high} stromal cells and *Pdgfra*-GFP^{medium} myofibroblasts within the S^{+}P^{+} population in sham and MI hearts (see Fig. 5G).

***In vivo* labelling of EdU, BrdU and tamoxifen induction**

BrdU (50mg/ml) and EdU (10 mg/ml) are delivered through subcutaneously implanted minipumps. 7-day pumps with a delivery rate of 0.5µl/ml were used for the 5 day assays, while 1µl/hr 2-week pumps were used for the 28 day assays with replacement pump insertions performed at the two weeks interval. For labelling of the

PDGFRa lineage positive cells *in vivo*, adult *Pdgfra-merCREmer x tdTomato* mice were given tamoxifen (40mg/ml, Sigma) via oral gavage (300mg/kg) for 2 days, MI surgeries were performed 1 week after the tamoxifen treatment, and hearts were subjected to IHC or FACS analysis at day 5 and day 28 post-MI surgeries.

Production of APA5 antibody

The blocking monoclonal antibody against PDGFRa was produced in house (Centre For Targeted Therapy, Garvan Institute of Medical Research) from the APA-5 hybridoma cell line [13, 14]. IgG was purified from the supernatant using Protein L Sepharose resin (Genscript) as previously described [15]and concentrated to 2mg/mL in PBS using an Amicon Ultra-15 Centrifugal filter unit (Millipore). The purity of the antibody preparation was validated by reducing and non-reducing SDS-PAGE and endotoxin contamination was assessed using the QCL-1000™ Endpoint Chromogenic LAL Assay (Lonza) according to manufacturer's instructions. Control IgG from Rat IgG2a isotype control clone 2A3 was sourced from BioXcell.

ELIZA assay

Serum was collected from 8wk old healthy and PDGF-AB-treated mice. Briefly, blood was collected via cardiac puncture after euthanasia and let clot at room temperature for 30mins before centrifugation at 1500rpm for 10mins. Serum concentration of mouse PDGF-AB and human PDGF-AB was measured using a Mouse/Rat PDGF-AB Quantikine ELISA Kit and a Human PDGF-AB Quantikine ELISA Kit (R&D Systems), respectively, following manufacturer's instructions and analysis using the ELISA Centro Luminescence Microplate Reader (*Bio-Rad).*

QUANTIFICATION AND STATISTICAL ANALYSIS

Statistical analyses of live cell tracking data were implemented in custom-written scripts in Matlab. Kaplan-Meier (KM) analysis was used to generate empirical cumulative distribution functions for cell division. Cox regression was used to test for group differences and to estimate the relative risk of division (relative to untreated controls). The relative frequency of observed fates in each treatment group was quantified by counting the number of cells with distinct fate outcomes in each group. Student's *t*-tests were used to test for significant differences in the proportion of observed fates in each treatment group. All Matlab code will be made available upon request. For all other data, Student's *t*-tests were used to determine significance between triplicate experiments.

DATA AND SOFTWARE AVAILABILITY

RAW and normalised microarray data are available at NCBI's Gene Expression Omnibus (GSE106778; GSE106779) [4].

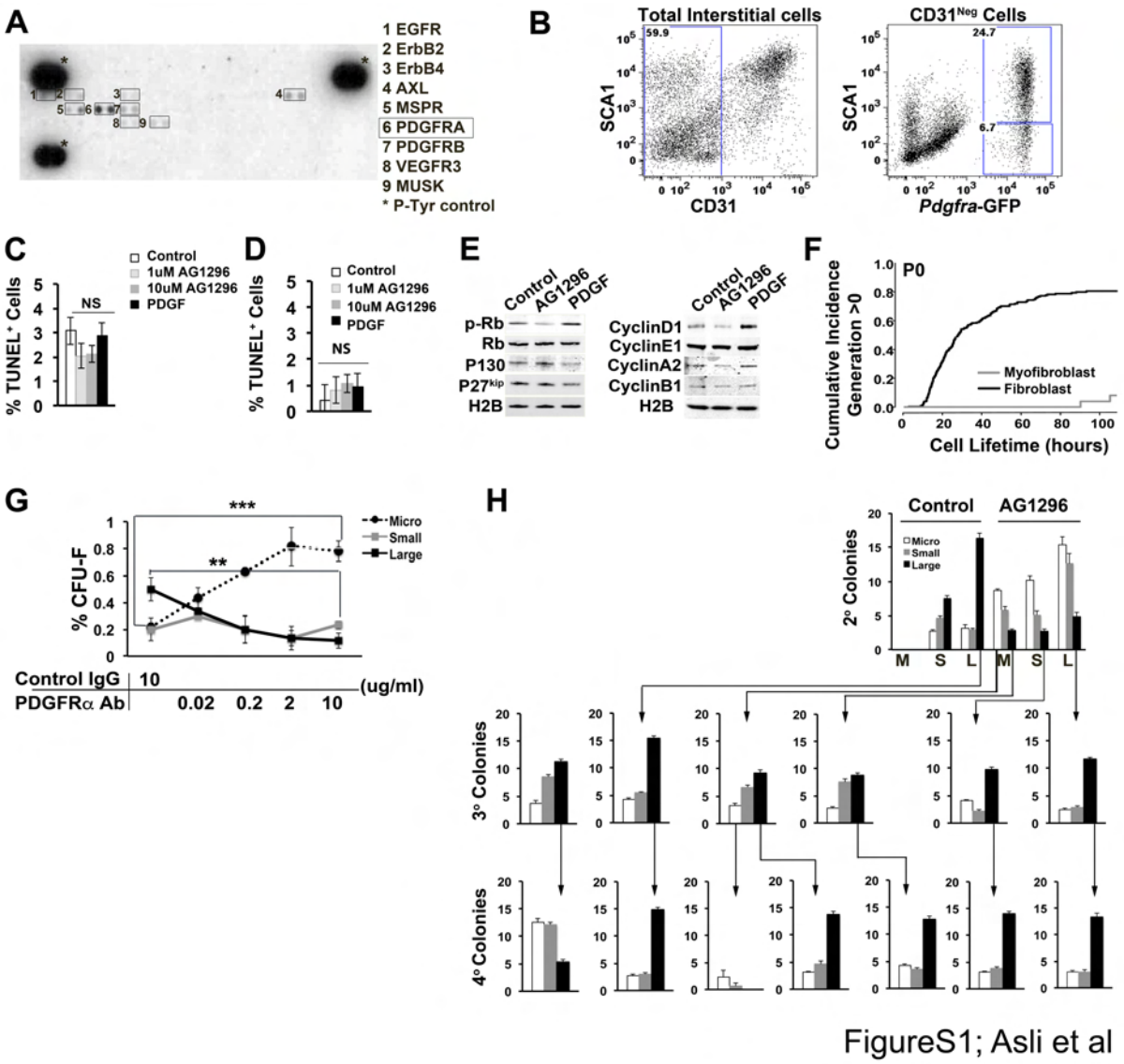

FigureS1; Asli et al

2. Supplementary Figures and Legend

Figure S1: Screen for tyrosine kinases active in S^+P^+ cultures, and cell cycle, cell death and colony-forming assays in AG1296 and PDGF-AB-treated cultures

(A) Membrane-based tyrosine kinase receptor activity assay detecting tyrosine phosphorylation of specific receptors within extracts of S^+P^+ cultures at P0. Boxes – activity above background. (B) Flow cytometry plots demonstrating $SCA1^+$ and $SCA1^-$ sub-fractions of *Pdgfra*-GFP^+CD31^- cells. (C,D) Percent TUNEL-positive cells in S^+P^+ cultures treated throughout P0 and P4, respectively, with vehicle (control), AG1296 (10μM) or PDGF-AB (100ng/ml) (see Fig. 1I). (E) Western blot analysis of cell cycle-associated proteins after treatment of S^+P^+ cultures across P4 with

AG1296 or PDGF-AB. (F) Accumulated proportion of plated S^+P^+ cells showing fibroblastic or myofibroblastic morphologies undergoing cell division (generations >0). (G) cCFU-F analysis of S^+P^+ cells incubated in the presence of control IgG antibody or blocking anti-PDGFRα antibody, scored at the end of P0. (H) Selected data from a serial clonal cCFU-F analysis of pooled large (L), small (S) and micro-colonies (M) initially arising from freshly plated S^+P^+ cells cultured in vehicle (control) or AG1296 until the end of P0. Graphs show secondary (2^0), tertiary (3^0) and quaternary (4^0) colony assays after cloned primary colonies were passaged until the end of P1, P2 and P3 in the absence of inhibitor.

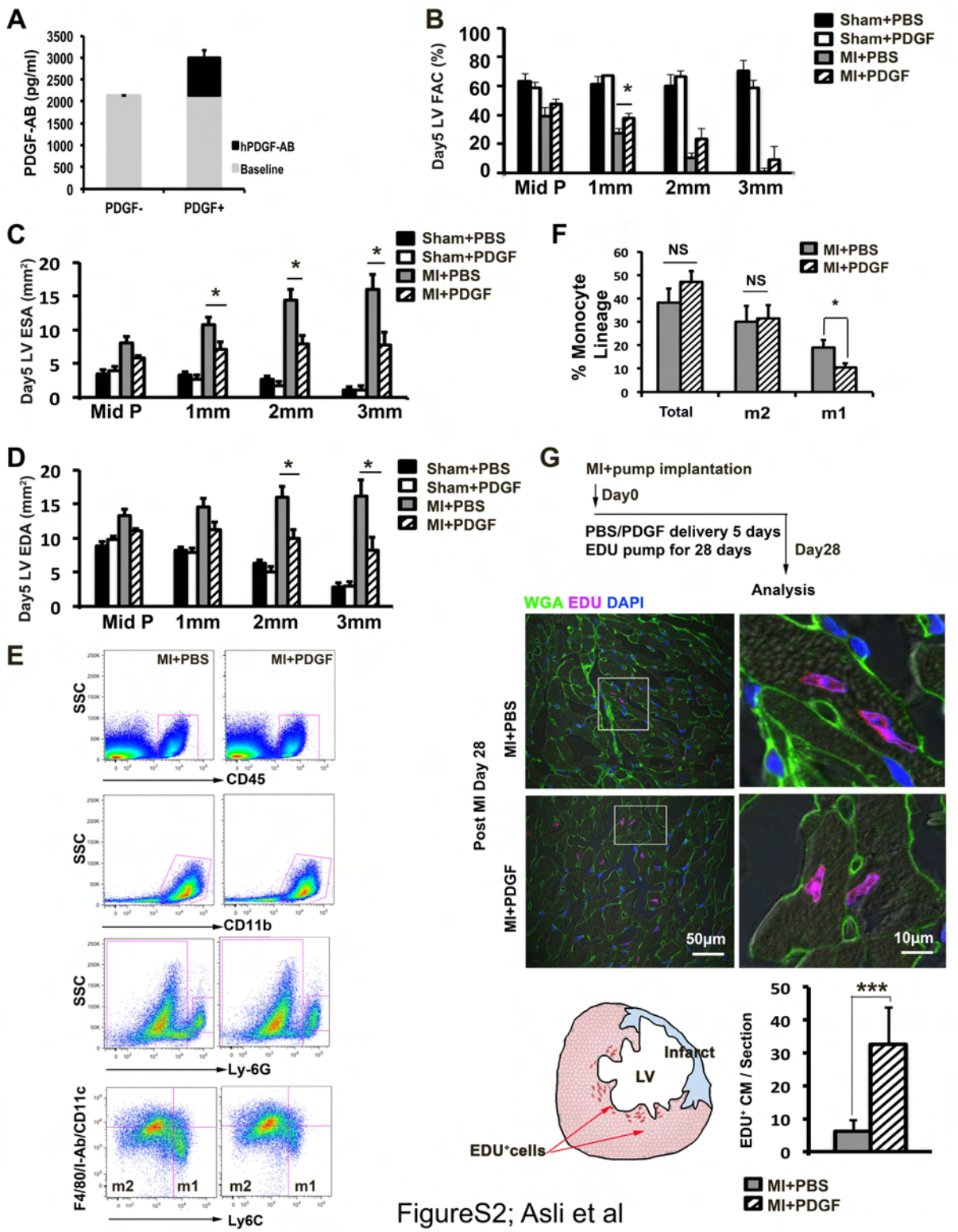

Figure S2: Quantification of serum PDGF-AB, additional cardiac functional analyses, monocyte quantification strategy and EdU incorporation studies

(A) Levels of mouse (baseline) and human (h) PDGF-AB detected in mice untreated or treated with exogenous human recombinant PDGF-AB, analyzed by ELISA. (B-D)

Quantification of functional parameters in MI+PDGF-AB hearts at day 5 post-surgery, compared to sham+PBS, sham+PDGF-AB and MI+PBS controls – fractional area change (FAC), left ventricular end systolic area (LV ESA), and left ventricular end diastolic area (LV EDA), respectively, at different echocardiographic planes (see Fig. 2E). (E) Flow cytometric analysis strategy using side scatter (SSC) and indicated antibodies applied to total interstitial cells from MI+PBS control and MI+PDGF-AB hearts used to define m1 and m2 monocyte fractions. (F) Quantification of total monocyte lineage population as well as m1 and m2 monocytes from MI+PBS control and MI+PDGF-AB hearts (see Fig. 2L). (G) EdU incorporation in cardiomyocyte nuclei of MI-PBS and MI-PDGF hearts, with map of localisation of positive cells and quantification. LV: left ventricle; WGA: wheat germ agglutinin staining. All comparisons: * $p<0.05$; *** $p<0.001$; NS: non-significant.

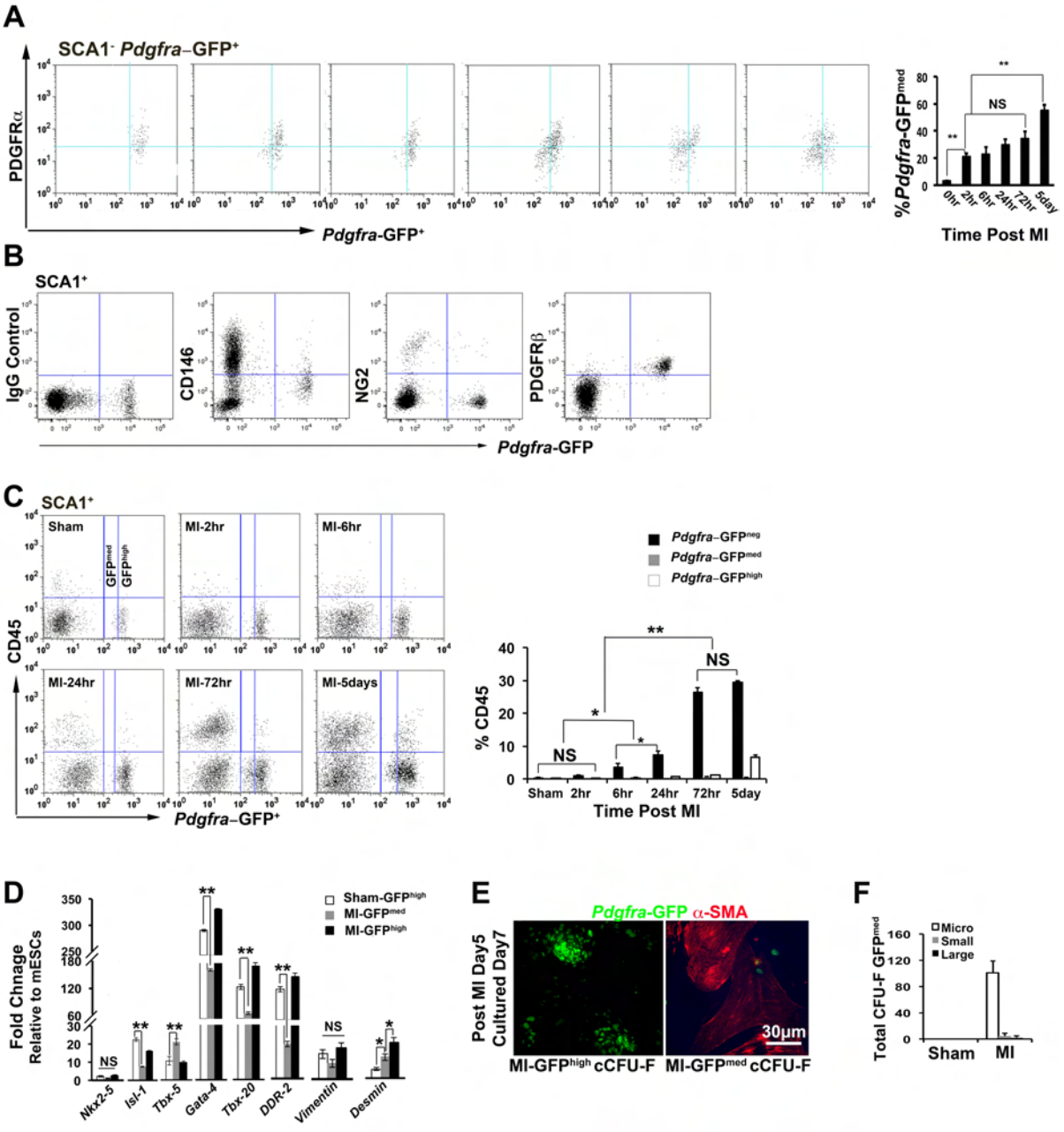

Figure S3; Asli et al

Figure S3: Flow cytometric analysis of pericyte and immune markers, and qRT-PCR quantification of gene expression, in SCA1$^+$ *Pdgfra*-GFP$^+$ fibroblasts

(A) Time course flow cytometry analysis of SCA1$^-$*Pdgfra*-GFP$^+$ fibroblasts, displaying PDGFRα and GFP expression, with quantification of GFP^{medium} myofibroblasts. (B) Flow cytometric analysis of indicated pericyte markers on cardiac SCA1$^+$ *Pdgfra*-

GFP^+ cells. (C) Flow cytometric analysis of CD45 and GFP expression in freshly isolated $SCA1^+$ cardiac interstitial cells from *Pdgfra*$^{GFP/+}$ mice with time after induction of myocardial infarction (MI), compared to cells from sham-operated mice. Graph indicates percent $CD45^+$ cells in $GFP^{negative}$, GFP^{medium} and GFP^{high} cardiac interstitial populations. (D) Quantitative RT-PCR analysis of indicated cardiac transcription factor and fibroblast markers in flow-purified GFP^{medium} and GFP^{high} cells from *Pdgfra*$^{GFP/+}$ mice subject to sham operation or MI. Fold change is relative to expression in undifferentiated mouse embryonic stem cells (mESCs). Most cardiac fibroblasts express cardiac transcription factor genes *Isl1, Gata4* and *Tbx20*, reflecting their epicardial origins and cardiac identity [16, 17]. However, S^+GFP^{medium} myofibroblasts showed reduced expression of these genes and of fibroblast markers vimentin and DDR-2. (E) Micrographs showing GFP fluorescence and α-SMOOTH MUSCLE ACTIN (α-SMA) immunofluorescence staining in 2 day cCFU-F cultures of flow-purified GFP^{medium} and GFP^{high} cells from *Pdgfra*$^{GFP/+}$ mice subject to MI (cells harvested at day 5 post-MI). S^+GFP^{medium} cells resembled myofibroblasts (large $GFP^{dim}SMA^{high}$ cells with evidence of actin stress fibres), whereas GFP^{high} cells were spindle-shaped, remained GFP^{bright} and were predominantly SMA^-. (F) cCFU-F analysis of GFP^{medium} population from sham and MI mice as defined in Fig. 3K. S^+GFP^{medium} cells formed only micro-colonies, which are typically composed of differentiated myofibroblast-like cells [1, 18]. All comparisons: * $p<0.05$; ** $p<0.01$. NS: non-significant.

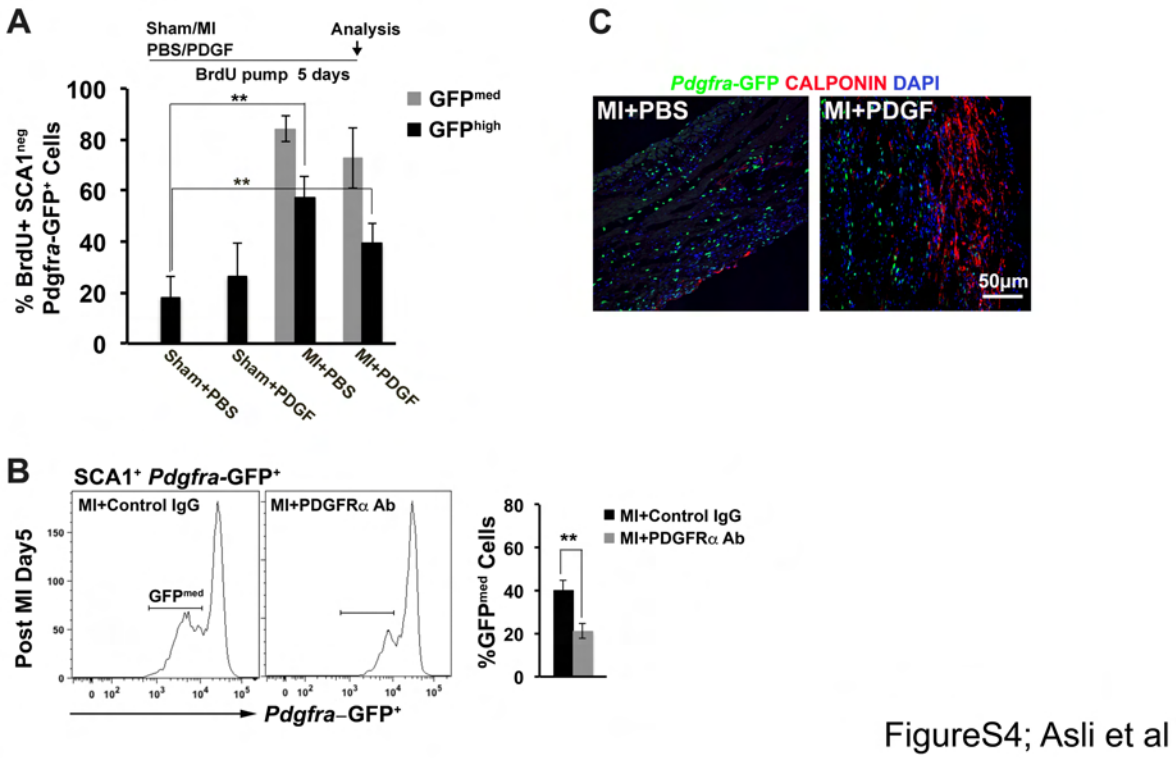

Figure S4: BrdU incorporation into SCA1$^-$ fibroblast, quantification of myofibroblasts and myofibroblast CALPONIN expression in sham and MI *Pdgfra*-GFP mice

(A) BrdU incorporation analysis of the SCA1$^-$ fraction of GFP$^+$ fibroblasts (GFP^{high}) and myofibroblasts (GFP^{med}) isolated from sham and MI *Pdgfra*$^{GFP/+}$ mice treated with PBS or PDGF-AB. (B) Flow cytometric analysis of SCA1$^+$*Pdgfra*-GFP$^+$ cardiac fibroblasts at day 5 post-MI after treatment with control IgG antibody or blocking PDGFRα antibody (Ab), with quantification of GFP^{medium} myofibroblasts (bar). (C) Micrographs showing GFP fluorescence and CALPONIN immunofluorescence in the infarct zone of *Pdgfra*$^{GFP/+}$ mice subject to MI. DAPI staining indicates nuclei. All comparisons: ** $p<0.01$.

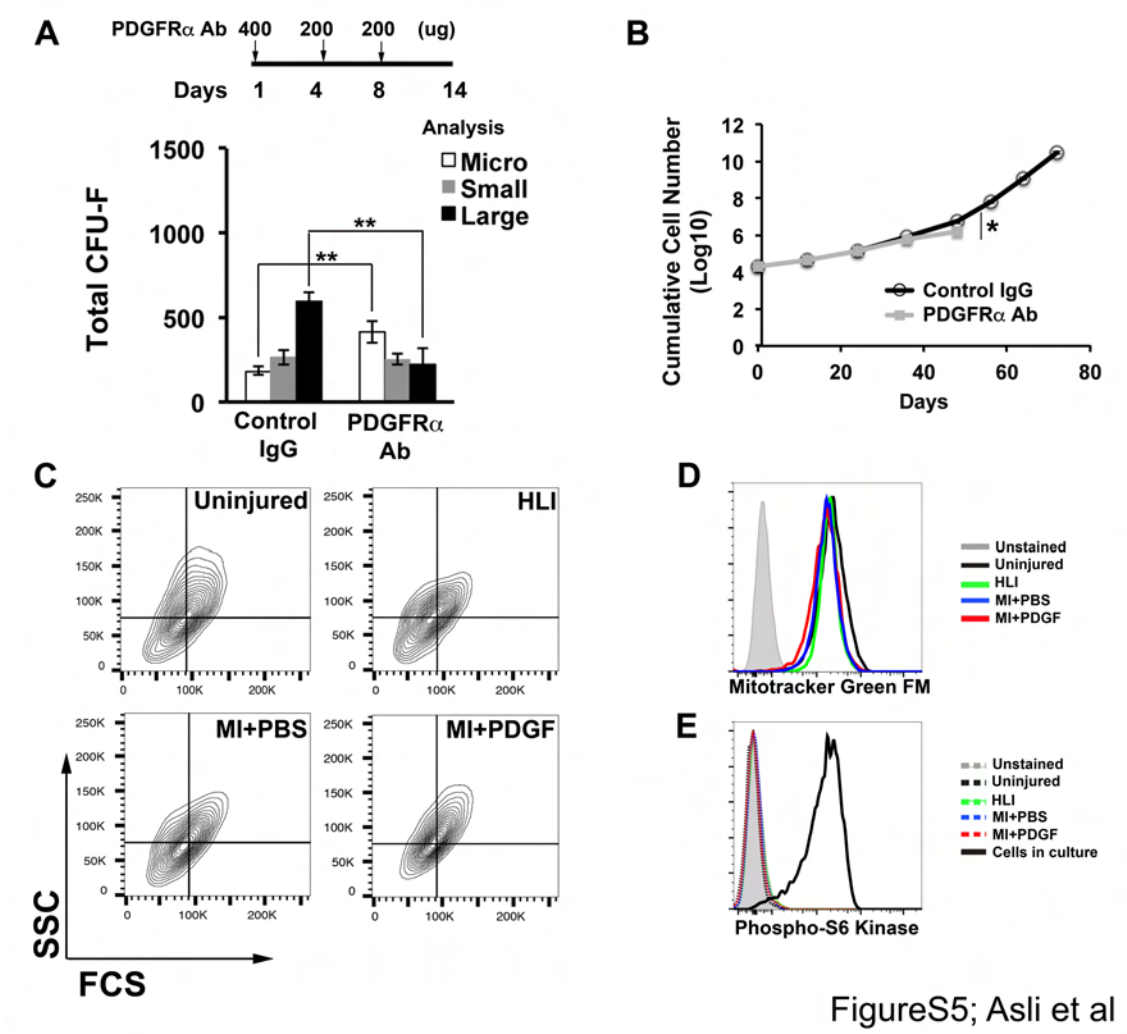

Figure S5: Inhibition of PDGFRα *in vivo* using blocking anti-PDGFRα antibody

(A) Treatment regime applicable to both control IgG or blocking PDGFRα (APA5) antibody, and graph of colony formation (cCFU-F) at day 14. (B) Long-term growth of S^+P^+ cultures from control IgG and APA5-treated animals initiated at day 14 post-treatment. (C-E) Flow cytometric analyses of cell size and granularity distribution (forward scatter, side scatter; C), mitochondrial content (Mitotracker Green FM staining; D) and Phospho-S6 Kinase expression in freshly-isolated S^+P^+ cells from uninjured animals, compared to those subject to hindlimb ischemic injury (HLI) or myocardial infarction (MI) after treatment with PBS or PDGF-AB. Analysis at 5 days post-injury. All comparisons: * $p<0.05$; ** $p<0.01$.

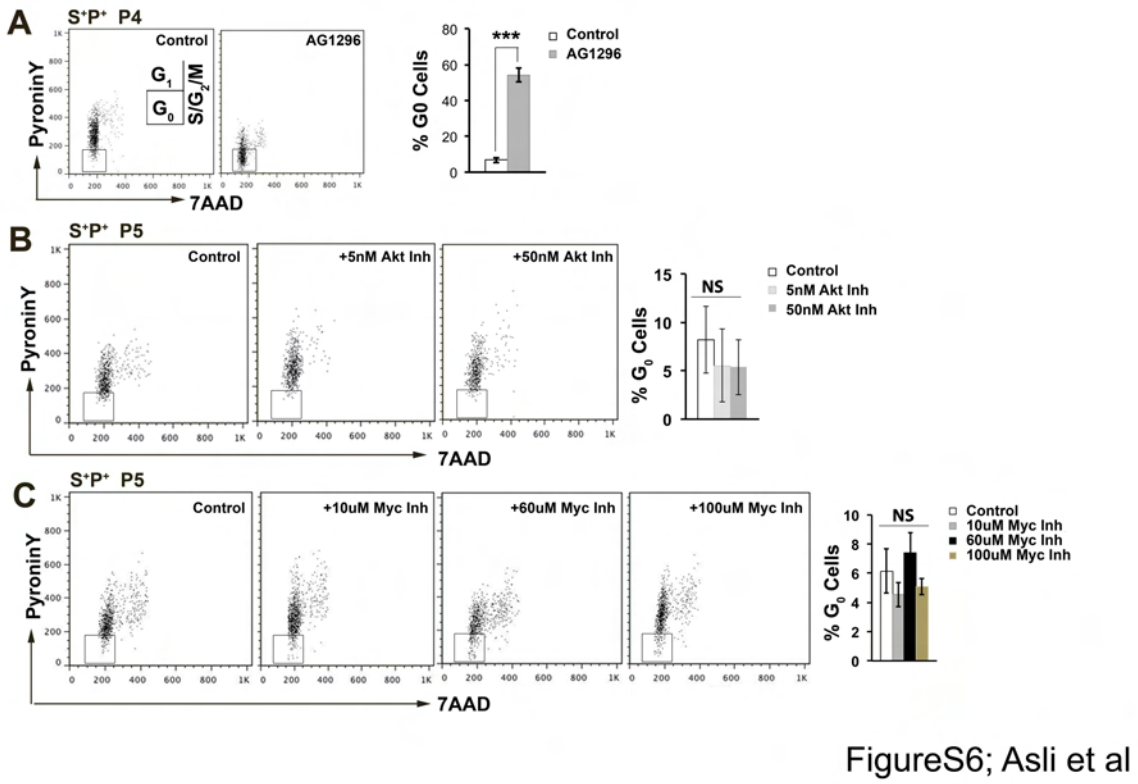

Figure S6: Signaling requirements of cCFU-F cultures

(A) Cell cycle analysis of S^+P^+ cultures treated with vehicle (control) or PDGFRα inhibitor AG1296 over P4 (see Fig. 6E,F). Graph shows percent cells in G_0 (boxed). (B,C) Cell cycle analysis and graph of percent cells in G_0 of S^+P^+ cultures treated across P5 with 5nM and 50nM AKT inhibitor (LY294002) or 10μM, 60μM, and 100μM MYC inhibitor 10058-F4, respectively, compared to vehicle (control). All comparisons: ** $p<0.01$; NS: non-significant.

3. References of the supplementary materials

1. Chong JJ, Chandrakanthan V, Xaymardan M, Asli NS, Li J, Ahmed I, Heffernan C, Menon MK, Scarlett CJ, Rashidianfar A, Biben C, Zoellner H, Colvin EK, Pimanda JE, Biankin AV, Zhou B, Pu WT, Prall OW and Harvey RP. Adult cardiac-resident MSC-like stem cells with a proepicardial origin. *Cell stem cell*. 2011;9:527-40.
2. Joun G and Asli NS. Cancer Cell Properties Shape Along Metabolic Activity in Human Epithelial Carcinoma. *Journal of Stem Cell: Advanced Research and Therapy* 2017;4:1-5.
3. Cornwell JA, Hallett RM, der Mauer SA, Motazedian A, Schroeder T, Draper JS, Harvey RP and Nordon RE. Quantifying intrinsic and extrinsic control of single-cell fates in

cancer and stem/progenitor cell pedigrees with competing risks analysis. *Sci Rep*. 2016;6:27100.
4. Edgar R, Domrachev M and Lash AE. Gene Expression Omnibus: NCBI gene expression and hybridization array data repository. *Nucleic Acids Res*. 2002;30:207-10.
5. Gentleman RC, Carey VJ, Bates DM, Bolstad B, Dettling M, Dudoit S, Ellis B, Gautier L, Ge Y, Gentry J, Hornik K, Hothorn T, Huber W, Iacus S, Irizarry R, Leisch F, Li C, Maechler M, Rossini AJ, Sawitzki G, Smith C, Smyth G, Tierney L, Yang JY and Zhang J. Bioconductor: open software development for computational biology and bioinformatics. *Genome Biol*. 2004;5:R80.
6. Huang da W, Sherman BT and Lempicki RA. Systematic and integrative analysis of large gene lists using DAVID bioinformatics resources. *Nat Protoc*. 2009;4:44-57.
7. Gautier L, Cope L, Bolstad BM and Irizarry RA. affy--analysis of Affymetrix GeneChip data at the probe level. *Bioinformatics*. 2004;20:307-15.
8. Stacklies W, Redestig H, Scholz M, Walther D and Selbig J. pcaMethods--a bioconductor package providing PCA methods for incomplete data. *Bioinformatics*. 2007;23:1164-7.
9. Smyth GK. limma: Linear Models for Microarray Data. In: R. Gentleman, V. J. Carey, W. Huber, I. R.A. and S. Dudoit, eds. *Bioinformatics and Computational Biology Solutions Using R and Bioconductor Statistics for Biology and Health* New York, NY: Springer; 2005.
10. Benjamini Y and Hochberg Y. Controlling the false discovery rate: a practical and powerful approach to multiple testing. *Journal of the Royal Statistical Society, Series B*. 1995;57:289-300.
11. Kageyama Y and Bravo EL. Hypertensive mechanisms associated with centrally administered aldosterone in dogs. *Hypertension*. 1988;11:750-3.
12. Brunner HR, Laragh JH, Baer L, Newton MA, Goodwin FT, Krakoff LR, Bard RH and Buhler FR. Essential hypertension: renin and aldosterone, heart attack and stroke. *The New England journal of medicine*. 1972;286:441-9.
13. Takakura N, Yoshida H, Kunisada T, Nishikawa S and Nishikawa SI. Involvement of platelet-derived growth factor receptor-alpha in hair canal formation. *J Invest Dermatol*. 1996;107:770-7.
14. Takakura N, Yoshida H, Ogura Y, Kataoka H, Nishikawa S and Nishikawa S. PDGFR alpha expression during mouse embryogenesis: immunolocalization analyzed by whole-mount immunohistostaining using the monoclonal anti-mouse PDGFR alpha antibody APA5. *J Histochem Cytochem*. 1997;45:883-93.
15. Dudgeon K, Rouet R, Kokmeijer I, Schofield P, Stolp J, Langley D, Stock D and Christ D. General strategy for the generation of human antibody variable domains with increased aggregation resistance. *Proc Natl Acad Sci U S A*. 2012;109:10879-84.
16. Furtado MB, Costa MW, Pranoto EA, Salimova E, Pinto AR, Lam NT, Park A, Snider P, Chandran A, Harvey RP, Boyd R, Conway SJ, Pearson J, Kaye DM and Rosenthal NA. Cardiogenic genes expressed in cardiac fibroblasts contribute to heart development and repair. *Circ Res*. 2014;114:1422-34.
17. Noseda M, Harada M, McSweeney S, Leja T, Belian E, Stuckey DJ, Abreu Paiva MS, Habib J, Macaulay I, de Smith AJ, al-Beidh F, Sampson R, Lumbers RT, Rao P, Harding SE, Blakemore AI, Jacobsen SE, Barahona M and Schneider MD. PDGFRalpha demarcates the cardiogenic clonogenic Sca1+ stem/progenitor cell in adult murine myocardium. *Nat Commun*. 2015;6:6930.
18. Cornwell JA, Nordon RE and Harvey RP. Analysis of cardiac stem cell self-renewal dynamics in serum-free medium by single cell lineage tracking. *Stem Cell Res*. 2018;28:115-124.

4. Resources table

REAGENT or RESOURCE	SOURCE	IDENTIFIER
Antibodies		

Rb	Abcam	ab6075-1
PhosphoRb (Ser780)	Cell Signaling	D59B7
P130	Abcam	76234
$P27^{kip}$	BD Biosciences	610242
H2B	Abcam	Ab18977
CyclinA2	Cell Signaling	4656P
CyclinB1	Cell Signaling	4138P
CyclinE1	Cell Signaling	4129P
CyclinD1	Cell Signaling	2978P
c-Myc	Santa Cruz	sc-788
Akt (pan-Akt)	Cell Signaling	4691
p-Akt308	Cell Signaling	2965
p-Akt473	Cell Signaling	4060
p-FOXO1	Cell Signaling	9461
FOXO1	Cell Signaling	2880
α- actinin	Sigma-Aldrich	A7811
NKX2-5	Santa Cruz	Sc-8697
WGA	Thermo Fisher Scientific	W11261
SMA	Sigma-Aldrich	A2547
eNOS	Abcam	ab66127
SM22	Abcam	ab14106
Calponin	Abcam	ab46794
Caveolin1	BD Biosciences	610059
CD31	BD Biosciences	553370
MyH11	Santa Cruz	6956)
MEF2C	Cell Signaling	5030S
pH3	Upstate	06-570
Ki67	Abcam	ab15580
BrdU	Abcam	ab6326
PDGFRα	Cell Signaling	3164
PDGFRβ	Santa Cruz	Sc-432
Lectin	Sigma-Aldrich	L3759
Isolectin	Thermo Fisher Scientific	I21411
Collagen IV	Abcam	ab19808
Collagen VI	Abcam	ab6588
cTnT	Thermo Fisher Scientific	MS-295-P1
Ly-6C PE	eBioscience	12-5932-80
F4/80 FITC	eBioscience	11-4801
CD11c FITC	BD Biosciences	553953
$I\text{-}A^b$ FITC	BD Biosciences	553456
PE Sca1 (Ly6A/E)	BD Biosciences	5531108
CD45- APCCy7	BD Biosciences	557659
CD31-PECy7	eBioscience	25-0311-82
PDGFRa (CD140a)-APC	eBioscience	17-1401-81
Ly-6G (Gr-1)-PerCPCy5	BD Biosciences	45-5931-80
CD11b-APC	BD Biosciences	553312
mPDGFRa	R&D System	AF1042
mPDGFRb	R&D System	AF1062
CD146	Abcam	Ab75769
NG2	EMD Millipore	AB5320

Bacterial and Virus Strains		
Biological Samples		
Chemicals, Peptides, and Recombinant Proteins		
PDGF-AB	R&D System	222-AB
AG1296	Cayman Chemical	146535-11-7
Imatinib	LC Laboratories	I-5508
cMyc inhibitor (10058-F4)	Sigma-Aldrich	F3680
Akt inhibitor (LY294002)	Cell Signaling	9901
PyroninY	Polysciences	18614-5
7AAD	BD Biosciences	51-68981E
Mitotracker Green FM	Thermo Fisher Scientific	M7514
Hoechst	Invitrogen	H369
DAPI	Thermo Fisher Scientific	62247
Aldosterone	Sigma-Aldrich	234362
Tamoxifen	Sigma-Aldrich	T5648
BrdU	Sigma-Aldrich	B5002
Alizarin Red S	Sigma-Aldrich	A5533
Oil Red O	Sigma-Aldrich	O0625
Alcian Blue	Sigma-Aldrich	A5268
Critical Commercial Assays		
Mouse Phospho-Receptor Tyrosine Kinase Array Kit	R&D Systems	ARY014
Click-iT EdU assay kit	Thermo Fisher Scientific	C10337
DeadEnd™ Colorimetric TUNEL System	Promega	G736
Masson Trichrome Staining kit	Sigma-Aldrich	HT-15
Mouse/Rat PDGF-AB Quantikine ELISA Kit	R&D Systems	MHD00
Human PDGF-AB Quantikine ELISA Kit	R&D Systems	DHD00C
Deposited Data		
https://www.ncbi.nlm.nih.gov/geo/query/acc.cgi?acc=GSE106779- reviewer token: ifczsmwwhzkfxwb	This paper	N/A
Experimental Models: Cell Lines		
Experimental Models: Organisms/Strains		
Mouse, Pdgfra-GFP, KI GFP, KO	Jackson Laboratory	*Pdgfra* $^{tm11(EGFP)Sor}$
Mouse, Pdgfra^{fl}, TG	Jackson Laboratory	B6.Cg-Pdgfratm8Sor/EiJ
Mouse, Nkx2-5 GFP, KI GFP, KO	Harvey laboratory	*B6.129S1(C)-Nkx2-5tm4Rph/J*
Mouse, β-Actin-GFP, TG	Jackson Laboratory	*Tg(CAG-EGFP)1Osb*
Mouse, PdRa-MCM, KI	RIKEN Center for Developmental Biology, Kobe, Japan	*Pdgfra-merCremer*
Mouse, tdTomato Red, TG	Jackson Laboratory (Imported from ARMI)	*B6.Cg-Gt(ROSA)26Sor*$^{tm14(CAG-tdTomato)Hze}$*/J*

Oligonucleotides		
Primer: PolG F:CACGGACCTCCTGCCTAAG R:TCATCTAGTCGAGGGGCAGAG	This paper	N/A
Primer: PolG2 F:AGCCAATAGAAACCCTGTGG R:CACTTACAGACAGAACGCAACG	This paper	N/A
Primer: Tfam F:TCAGGAGGCAGTTATTG R:CAGGAAGTCTTCACGTTGACC	This paper	N/A
Primer: Smooth Muscle Actin F:GCTGACAGAGGCACCACTGA R:CATCTCCAGAGTCCAGCACA	This paper	N/A
Primer: Calponin F:GAACCCTGTGGACCTGTTTGA R:GCGTCGTCAAAGTTCCTCTC	This paper	N/A
Primer: Embryonic Smooth Muscle F:CGCTTTGGCAAGTTTATCCG R:CAGCACTGAAGACACGACTT	This paper	N/A
Primer: Fibronectin (EIIA) F:CCCACTGTGGAGTACGTGG R:GAGTCCTGACACAATCACCG	This paper	N/A
Primer: Fibronectin (EIIB) F:GGGGACCTCTCTGGAAGAAGTGG R:GTCCCAGGCAGGAGATTTG	This paper	N/A
Primer: Nkx2-5 F:CCCAAGTGCTCTCCTGCTTTC R:TCCAGCTCCACTGCCTTCTG	This paper	N/A
Primer: Islet-1 *Primer:* F:TCATCCGAGTGTGGTTTCAA R:CCATCATGTCTCTCCGGACT	This paper	N/A
Primer: Tbx-5 *Primer:* F:ATGGTCCGTAACTGGCAAAG R:TTTCGTCTGCTTTCACGATG	This paper	N/A
Primer: Gata-4 F:GCCCGGGCTGTCATCTCACTATG R:GCTGGCCTGCGATGTCTGAGTG	This paper	N/A
Primer: Tbx-20 F:GCAGCAGAGAACACCATCAA R:CAGAGCTCCTTCGTTTCCAG	This paper	N/A
Primer: DDR-2 F:CTGTCGGATGAGCAGGTTAT R:CTCGGCTCCTTGCTGAAGAA	This paper	N/A
Primer: Vimentin F:TACCAGGACACTATTGGCCG *Primer:* R:CTGTTGCACCAAGTGTGTGC	This paper	N/A
Primer: Desmin F:GCTATCAGGACAACATTGCG R:GTTGTTGCTGTGTAGCCTCG	This paper	N/A
Primer: mTR F:GCTGTGGGTTCTGGTCTTTT R:CGTTTGTTTTTGAGGCTCGG	This paper	N/A
Primer: mTERT F:CCAACACTGTTATTGAGACCCTG R:GGCCTGTAACTAGCGGACACA	This paper	N/A
Primer: GusB *Primer:* F:CCTTCTAGCTTCAATGACATC R:GATCCTCAACACCACTCTC	This paper	N/A
Primer: 18S rRNA	This paper	N/A

F:AGGGGAGAGCGGGTAAGAGA R:GGACAGGACTAGGCGGAACA		
Primer: GAPDH F:GGTCCTCAGTGTAGCCCAAG R:AATGTGTCCGTCGTGGATCT	This paper	N/A
Primer: HPRT F:AGTGTTGGATACAGGCCAGAC R:CGTGATTCAAATCCCTGAAGT	This paper	N/A
Recombinant DNA		
Software and Algorithms		
Other		